Direct Measurements of Covalently Bonded Sulfuric Anhydrides from Gas-Phase Reactions of SO_3 with Acids under Ambient Conditions

Kumar, Avinash; Iyer, Siddharth; Barua, Shawon; Brean, James; Besic, Emin; Seal, Prasenjit; Dall'Osto, Manuel; Beddows, David C.S.; Sarnela, Nina; Jokinen, Tuija; Sipilä, Mikko; Harrison, Roy M.; Rissanen, Matti

DOI:
10.1021/jacs.4c04531

Document Version
Publisher's PDF, also known as Version of record

Citation for published version (Harvard):
Kumar, A, Iyer, S, Barua, S, Brean, J, Besic, E, Seal, P, Dall'Osto, M, Beddows, DCS, Sarnela, N, Jokinen, T, Sipilä, M, Harrison, RM & Rissanen, M 2024, 'Direct Measurements of Covalently Bonded Sulfuric Anhydrides from Gas-Phase Reactions of SO_3 with Acids under Ambient Conditions', *Journal of the American Chemical Society*, vol. 146, no. 22, pp. 15562-15575. https://doi.org/10.1021/jacs.4c04531

JACS
JOURNAL OF THE AMERICAN CHEMICAL SOCIETY
pubs.acs.org/JACS
Article

Direct Measurements of Covalently Bonded Sulfuric Anhydrides from Gas-Phase Reactions of SO_3 with Acids under Ambient Conditions

Avinash Kumar,*,○ Siddharth Iyer,*,○ Shawon Barua, James Brean, Emin Besic, Prasenjit Seal, Manuel Dall'Osto, David C. S. Beddows, Nina Sarnela, Tuija Jokinen, Mikko Sipilä, Roy M. Harrison, and Matti Rissanen*

Cite This: J. Am. Chem. Soc. 2024, 146, 15562−15575

ABSTRACT: Sulfur trioxide (SO_3) is an important oxide of sulfur and a key intermediate in the formation of sulfuric acid (H_2SO_4, SA) in the Earth's atmosphere. This conversion to SA occurs rapidly due to the reaction of SO_3 with a water dimer. However, gas-phase SO_3 has been measured directly at concentrations that are comparable to that of SA under polluted mega-city conditions, indicating gaps in our current understanding of the sources and fates of SO_3. Its reaction with atmospheric acids could be one such fate that can have significant implications for atmospheric chemistry. In the present investigation, laboratory experiments were conducted in a flow reactor to generate a range of previously uncharacterized condensable sulfur-containing reaction products by reacting SO_3 with a set of atmospherically relevant inorganic and organic acids at room temperature and atmospheric pressure. Specifically, key inorganic acids known to be responsible for most ambient new particle formation events, iodic acid (HIO_3, IA) and SA, are observed to react promptly with SO_3 to form iodic sulfuric anhydride (IO_3SO_3H, ISA) and disulfuric acid ($H_2S_2O_7$, DSA). Carboxylic sulfuric anhydrides (CSAs) were observed to form by the reaction of SO_3 with C_2 and C_3 monocarboxylic (acetic and propanoic acid) and dicarboxylic (oxalic and malonic acid)−carboxylic acids. The formed products were detected by a nitrate-ion-based chemical ionization atmospheric pressure interface time-of-flight mass spectrometer (NO_3^--CI-APi-TOF; NO_3^--CIMS). Quantum chemical methods were used to compute the relevant SO_3 reaction rate coefficients, probe the reaction mechanisms, and model the ionization chemistry inherent in the detection of the products by NO_3^--CIMS. Additionally, we use NO_3^--CIMS ambient data to report that significant concentrations of SO_3 and its acid anhydride reaction products are present under polluted, marine and polar, and volcanic plume conditions. Considering that these regions are rich in the acid precursors studied here, the reported reactions need to be accounted for in the modeling of atmospheric new particle formation.

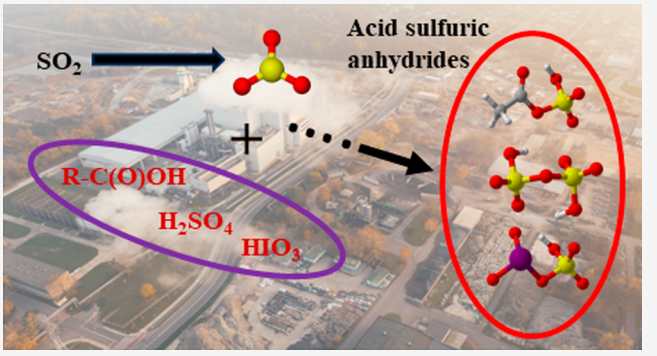

1. INTRODUCTION

Sulfur oxides (SO_x) are major air pollutants that contribute to acid rain and particulate matter formation in the Earth's atmosphere.[1−3] Among the SO_x, sulfur dioxide (SO_2) is the most emitted, with burning of fuels and human activities being the dominant source along with natural emission processes.[4−6] Sulfur trioxide (SO_3) is formed by the gas-phase oxidation of SO_2 and is an important intermediate toward the formation of sulfuric acid (SA, H_2SO_4), which plays a key role in atmospheric new particle formation (NPF).[7−10] These oxides of sulfur can also react on organic surfaces generating organosulfates (OS), which affect the physicochemical properties of aerosol particles.[11−16] The aerosol particles in the atmosphere are well-known to influence climate, air quality, and human health.[17−22] Numerous field measurements have shown that OS are present in atmospheric particles in concentrations high enough to affect atmospheric physicochemical processes.[13,23−25] It has been estimated that OS contribute to up to 30 and 12% of the organic mass and total sulfur, respectively, at a forest site in Hungary.[26,27]

Carboxylic acids comprise a major fraction of the organics present in the atmosphere[17,27,28] and are largely sourced from photo-oxidation of vehicle emissions and biomass burning.

Received: April 2, 2024
Revised: April 22, 2024
Accepted: April 23, 2024
Published: May 21, 2024

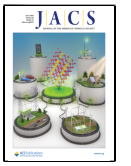

They can also be directly emitted by vegetation and from cooking.[17,28−34] They are observed both in the gas and particle phases and are known to stabilize the prenucleation clusters by binding strongly with other species in the atmosphere.[35−40] The concentration of acetic acid was measured to be in the range of 1.5−8.4 × 10^{10} molecules cm^{-3} in northwestern USA and 0.5−43.8 × 10^{10} molecules cm^{-3} at an urban site in California.[41,42] Among dicarboxylic acids, oxalic acid is the most prevalent, with concentrations ranging from 10^7 to 10^9 molecules cm^{-3} in urban and nonurban atmospheres.[43−46] In certain remote locations, carboxylic acids can account for as much as 80−90% of acidity in the precipitation.[47,48] They can also contribute to the formation of cloud condensation nuclei.[49,50] SA and iodic acid (IA) are well-known drivers of tropospheric nucleation processes.[8,10,51−65] Daytime SA concentrations are estimated to be in the range of 10^6−10^7 molecules cm^{-3} or below in most urban and remote locations and it can even reach up to 10^8 molecules cm^{-3} in polluted environments.[66−69] The concentration of IA in the polluted urban environment of Beijing and Nanjing reaches up to 10^6 molecules cm^{-3} in the summer months.[70] The IA concentration sourced by biogenic emissions near coastal environments can even reach up to 10^8 cm^{-3}.[59,71,72]

Only a few studies have investigated the gas-phase formation mechanism of organosulfur compounds from the reactions of SO_3 with organics present in the atmosphere. As the atmospheric lifetime of gaseous SO_3 is traditionally thought to be extremely short due to its fast reaction with the water dimer (to produce SA), its reaction with other atmospherically relevant species is not well studied. However, Yao et al.[73] recently measured appreciable levels of SO_3 during the winter (∼4 × 10^4−1.9 × 10^6 molecules cm^{-3}) and summer months (∼5 × 10^3−1.4 × 10^5 molecules cm^{-3}) in urban Beijing, using a nitrate-chemical ionization atmospheric pressure interface-long-time-of-flight (nitrate-CI-APi-LTOF) mass spectrometer. This indicates that significant steady-state concentrations of gaseous SO_3 could exist under the polluted conditions of mega-cities.

Mackenzie et al.[74] performed laboratory experiments and theoretical calculations to study the reaction of formic acid with SO_3 under supersonic jet conditions, with the products characterized by Fourier transform microwave (FTMW) spectroscopy. They reported that the reaction produces a covalently bonded formic sulfuric anhydride (FSA) product formed by the cycloaddition of SO_3 to formic acid. Subsequent experimental studies from the same laboratory have similarly used FTMW spectroscopy to report the formation of carboxylic sulfuric anhydrides (CSAs) from the reaction of SO_3 with acetic, acrylic, trifluoroacetic, propiolic, and pivalic acids.[75−79] Liu et al.[80] carried out computational calculations for the reaction of SO_3 with methanol to form methyl hydrogen sulfate and reported it to be competitive with the formation process of SA in dry and polluted regions and can reduce SA concentration up to 87%. Li et al.[81] studied the formation of sulfamic acid from the reaction of SO_3 with ammonia (NH_3) and reported that the energy barrier of SO_3−NH_3 reaction gets lowered upon NH_3 acting as a self-catalyst. It is a competitive loss pathway for SO_3 when compared to the conventional SO_3−H_2O system in dry and highly polluted regions with relatively higher concentrations of ammonia. Sarkar et al.[82] also calculated the catalytic effect of water and NH_3 on SO_3−NH_3 and SO_3−H_2O reaction systems. They reported that the NH_3-catalyzed pathway is faster than the H_2O-catalyzed pathway for both systems, and NH_3-catalyzed ammonolysis of SO_3 shows a higher rate coefficient than NH_3-catalyzed hydrolysis reaction of SO_3. Long et al.[83] studied the reaction of nitric acid (HNO_3) with SO_3 to form $HOSO_2$−NO_3 as a product, which has implications for understanding the sulfur partitioning in the stratosphere. Their kinetic calculations indicate that the SO_3−HNO_3 reaction system is competitive with the SO_3−H_2O system and is two times higher than the $HONO_2$−OH reaction system in the altitude range of 25−35 km. Some recent theoretical studies report that the reactions of SO_3 with other acids such as dicarboxylic, tricarboxylic, and aromatic carboxylic acids are kinetically feasible and competitive.[84−89] This variety of CSAs was found to form more stable clusters with atmospheric nucleation agents such as SA, NH_3, and dimethyl amine compared to their respective acid precursors, which suggests it to be a potential participator in NPF.[84−89] There is only one computational study that reports the formation of disulfuric acid from the reaction of SA with SO_3 and its role in aerosol particle formation in the gas phase and air−water interface.[90]

To the best of our knowledge, there are only six experimental studies that report the formation of CSA from the reaction of SO_3 with carboxylic acids, but none under the actual ambient temperature and pressure conditions of the real atmosphere.[74−79] These experiments were performed under supersonic expansion where the samples were mixed at higher pressure (usually more than 1 atm), and characterization was performed in low-temperature and -pressure conditions.

In this work, we carried out the reaction of SO_3 with monocarboxylic acids (acetic acid (AA) and propionic acid (PA)), dicarboxylic acids (oxalic acid (OA) and malonic acid (MA)), SA, and IA in a laminar flow tube at atmospheric pressure and room temperature and monitored the products using a chemical ionization atmospheric pressure interface time-of-flight mass spectrometer with nitrate reagent ion (NO_3^--CI-APi-TOF, henceforth NO_3^--CIMS). This study is the first experimental demonstration of the formation and detection of disulfuric acid (DSA) and iodic sulfuric anhydride (ISA) under atmospherically relevant conditions of temperature and pressure in the gas phase. Additionally, an identification of IO_2SO_3H (i.e., iodous acid sulfate, HIO_2−SO_3) was made during the experiments with the HIO_3−SO_3 system. This work is a combined experimental and computational approach to understanding the interaction of SO_3 with several of the prevalent organic and inorganic species in the atmosphere.

2. METHODOLOGY

2.1. Experimental Setup. A NO_3^--CIMS instrument was used to detect the formed CSAs, DSA, and ISA.[69,91] The experiments were performed in a borosilicate glass flow tube reactor (length = 100 cm and i.d. = 5 cm) coupled to the NO_3^--CIMS. All of the experiments were performed at a laminar flow condition at room temperature and 1 atm pressure using zero air as a bath gas. The residence time for the chemical species to react in the flow tube was estimated to be around 11 s. SO_3 was produced in situ by the reaction of SO_2 with OH radicals or stabilized Criegee intermediate (sCI) in the presence of oxygen. The OH radicals and sCI were produced by the reaction of tetramethylethylene (TME, C_6H_{12}) with ozone. The flows of the gases were set by means of calibrated mass flow controllers, which were further utilized to calculate the concentration of a chemical species in

https://doi.org/10.1021/jacs.4c04531
J. Am. Chem. Soc. 2024, 146, 15562−15575

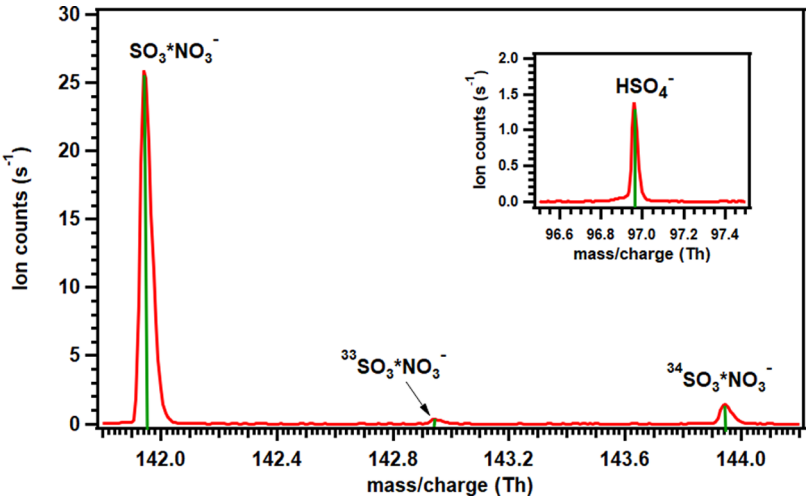

Figure 1. Mass spectra showing the formation of SO_3 in the reaction system.

the reaction mixture. Water was added to the reaction system to convert the formed SO_3 to SA, which shows that the latter plays no role in the formation of the sulfuric anhydride products. A more detailed explanation of the inlet flows, chemical system, concentration of the reactants, and the overall experimental setup is given in the Supporting Information (S1.1−S1.3).

2.2. Theoretical Methods. Systematic conformational sampling was carried out using the molecular mechanics Merck-Molecular-Force-Field (MMFF) methods with the Spartan '18 and '20 programs (Wavefunction, Inc.).[92−94] The generated conformers were optimized using density functional theory (DFT) methods, first at the low B3LYP/6-31+G(d) level of theory and later at the more accurate ωB97X-D/aug-cc-pV(T+d)Z level of theory for conformers within 2 kcal/mol of the lowest conformer in relative electronic energies. The DFT calculations were carried out using the Gaussian 16 program.[95] Transition-state (TS) geometries were found by optimizing guess structures with the bond distances corresponding to the TS constrained, followed by unconstrained TS optimizations. Once the correct TS geometry was found, a conformational sampling step was carried out with the TS-associated bond distances constrained, followed by constrained and TS optimizations. The energies of the lowest energy reactant, reaction complex, TS, and product structures were refined by recalculating their single-point electronic energies at the RHF-RCCSD(T)-F12a/VDZ-F12 level using the Molpro 2022.2.2 program.

Binding energies of the acid sulfuric anhydrides-NO_3^- clusters were calculated by performing systematic conformer sampling of the acid sulfuric anhydride molecule, its associated deprotonated form, and the cluster. Identical steps of low-level and higher-level DFT geometry optimizations were followed as previously. The final single-point electronic energy correction was performed using the DLPNO−CCSD(T)/Def2-QZVPP method as the DLPNO method has been shown previously to compare well with measurements for cluster binding energies.[96]

The temperature-dependent rate coefficients were calculated using the master equation solver for multienergy well reaction (MESMER) program.[97] The formation of reactive complexes (RCs) was treated using the MesmerILT method with a pre-exponential factor of 2×10^{-10} cm^3 molecule^{-1} s^{-1} and a modified Arrhenius parameter of 0.1. For the RC, an average energy transfer per collision with bath gas, E_{down}, of 225 cm^{-1} was used, which is within the MESMER recommended range of 175−275 cm^{-1} for N_2. The SimpleRRKM method was used for the formation of the sulfuric anhydride products, which were treated as "sink" during the simulations. The MESMER input and output files are provided as Supporting Files.

3. RESULTS AND DISCUSSION

3.1. Formation and Detection of SO_3 in Experiment. SO_3 is not commercially available, and therefore it was produced in situ in the flow reactor by the reaction of SO_2 with OH radical and sCI. OH radical and sCI ($C_3H_6O_2$) were produced in situ by the reaction of TME with ozone, along with acetone as a side product (R1)[98,99]

$$\mathrm{TME} + \mathrm{O_3} \rightarrow \mathrm{OH} + \mathrm{sCI} \quad \text{(R1)}$$

SO_2 can react with produced OH and sCI to form SO_3 in the presence of oxygen via reactions R2−R4[100−103]

$$\mathrm{SO_2} + \mathrm{OH} \rightarrow \mathrm{HOSO_2} \quad \text{(R2)}$$

$$\mathrm{HOSO_2} \xrightarrow{\mathrm{O_2}} \mathrm{SO_3} + \mathrm{HO_2} \quad \text{(R3)}$$

$$\mathrm{SO_2} + \mathrm{sCI} \rightarrow \mathrm{SO_3} + (\mathrm{CH_3})_2\mathrm{C{=}O} \quad \text{(R4)}$$

The formed SO_3 was directly detected by NO_3^--CIMS as $SO_3{*}NO_3^-$ cluster with a nominal mass-to-charge ratio of 141.9452 Th (see Figure 1). Peaks corresponding to other sulfur (^{33}S and ^{34}S) isotopes,[104] i.e., $^{33}SO_3{*}NO_3^-$ and $^{34}SO_3{*}NO_3^-$ with the nominal mass-to-charge ratio of 142.9446 and 143.9410 Th, respectively, were also measured.

We also observed trace levels of SA in our spectra with signals that were generally around 15 times lower than those of $SO_3{*}NO_3^-$. The formation of SA may be due to the reaction of SO_3 with water, which could have either formed chemically (from H-abstraction reactions of OH radicals with, e.g., precursor acids, TME, or acetone) or was present on the reactor surfaces or in the gas lines. The flows and concentrations in the chemical system were optimized to get a maximum signal of SO_3 and the minimum possible of SA. The final concentrations of SO_2, TME, and ozone were maintained at 2.73×10^{15}, 2.89×10^{11}, and 1.67×10^{11} molecules cm^{-3}, respectively. The same concentrations of

https://doi.org/10.1021/jacs.4c04531
J. Am. Chem. Soc. 2024, 146, 15562−15575

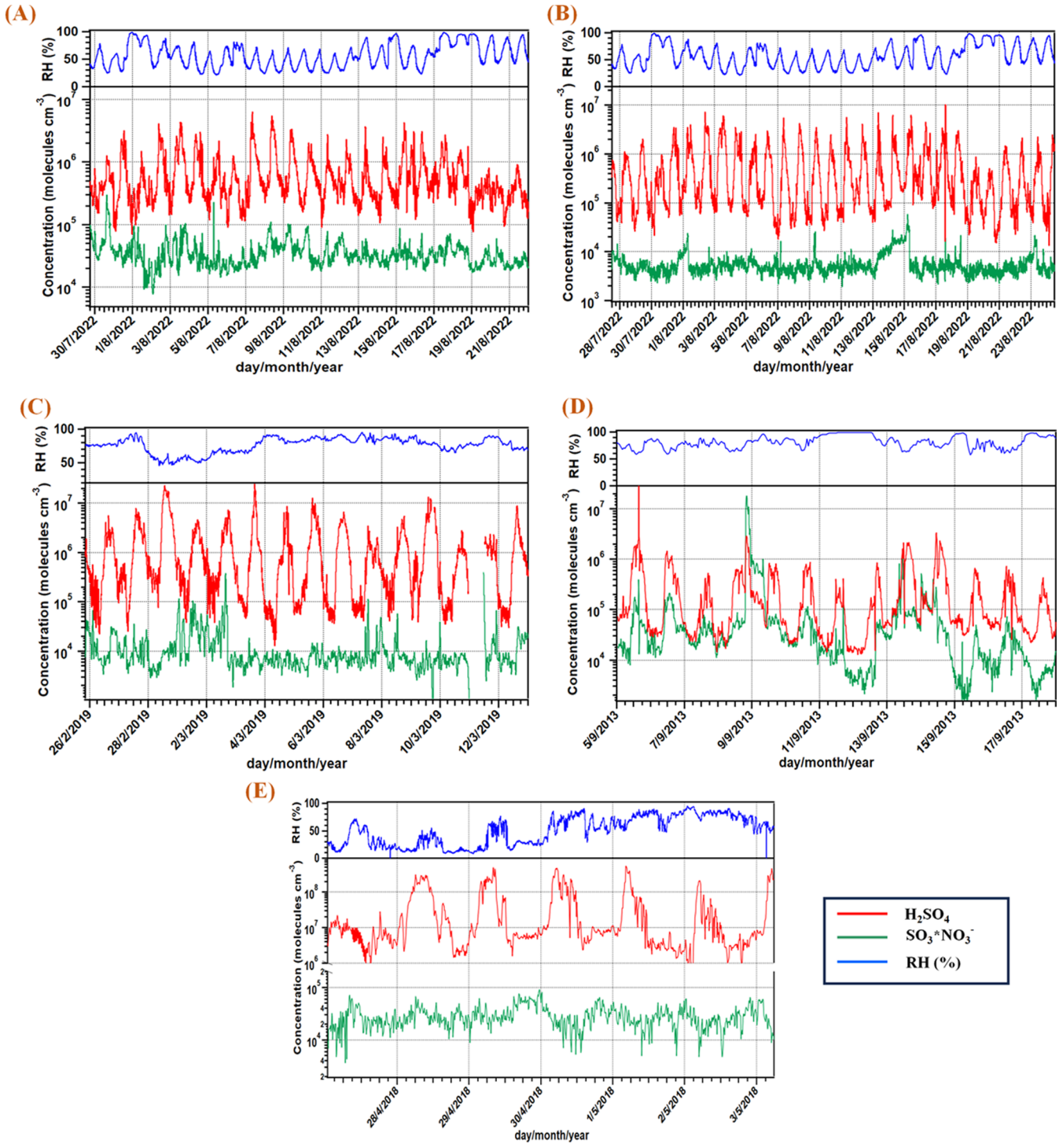

Figure 2. Time series plots showing the variation in the concentration of SO_3 and H_2SO_4 at contrasting chemical environments: (A) urban roadside site measurement station in Leipzig, Germany; (B) urban background site measurement station located at TROPOS, Leipzig, Germany; (C) Spanish research station Juan Carlos I, Antarctic Peninsula; (D) Mace Head research station, Ireland; and (E) Maïdo Observatory, Réunion island. All of the signals are normalized to the reagent ion signals. High-resolution peak fits of the individual products (SO_3*NO_3^-, HSO_4^-, and HNO_3*HSO_4^-) are shown in the Supporting Information (Figures S14−S18). The concentration of H_2SO_4 in the Mace Head research station (D) is from the contribution of the HNO_3*HSO_4^- signal only due to an overlapping peak in the HSO_4^- signal (see Section S1.5.4 in the Supporting Information), whereas for all other locations, both the signals of HSO_4^- and HNO_3*HSO_4^- are taken into account.

these three SO_3 precursors were used for all of the experiments. To detect the produced SO_3 with nitrate ionization, Yao et al.[73] have calculated the electronic binding energy of SO_3*NO_3^- to be −44.4 kcal mol^{-1}, which is substantially higher than that of HNO_3*NO_3^- (−29.2 kcal mol^{-1}), leading to efficient detection by NO_3^--CIMS.[105] Therefore, nitrate ionization was used in this study to detect SO_3 as well as the reaction products.

3.2. Ambient Field Measurement of SO_3. Gas-phase SO_3 was observed at various locations, spanning from urban

https://doi.org/10.1021/jacs.4c04531
J. Am. Chem. Soc. 2024, 146, 15562−15575

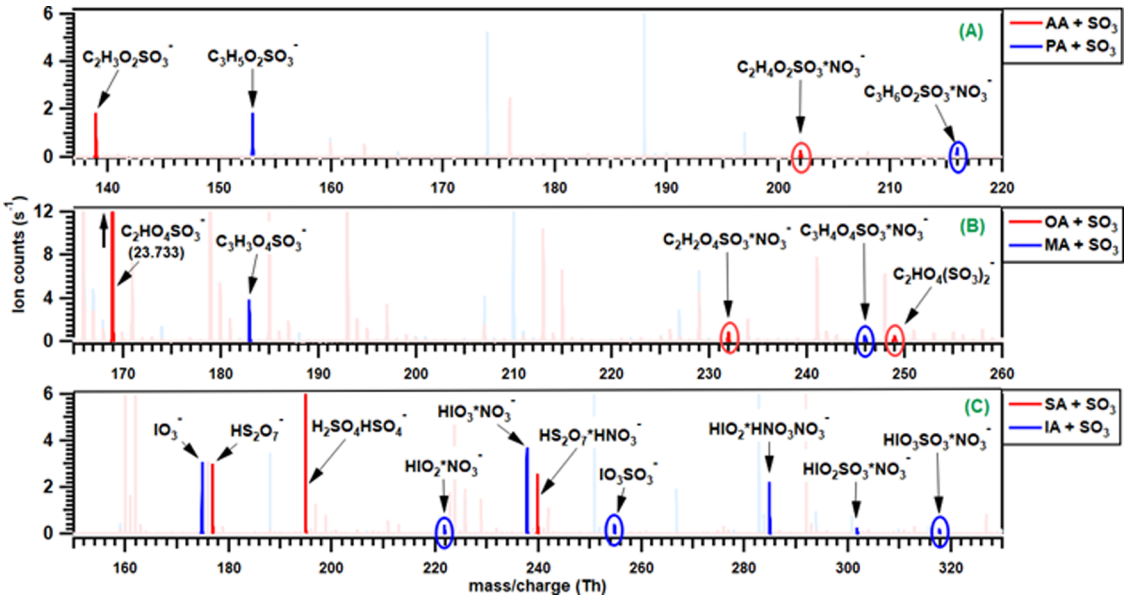

Figure 3. NO_3^--CIMS mass spectra obtained in the reaction of SO_3 with monocarboxylic acids (AA and PA) (panel A), dicarboxylic acids (OA and MA) (panel B), and inorganic acids (SA and IA) (panel C). The signals shown with a lower intense color in the background are the unidentified peaks. Note the different scales of the *y*-axes and the different mass range coverages. High-resolution peak fitting for all of the product peaks is given in the Supporting Information (Figure S13). Note that each of these mass spectra was obtained individually, with only one acid present at a time.

roadside and background sites in Leipzig, Germany, the polar Spanish research station Juan Carlos I in Antarctica, the marine Mace Head research station at coastal Ireland, and also the Maïdo Observatory located on Réunion island during volcanic plume conditions. The descriptions of these research locations are comprehensively detailed in the Supporting Information (S1.5). Measurement of SO_3 was performed by NO_3^--CIMS, and the diurnal profiles of SO_3 and SA concentrations during the select days at the different measurement sites are shown in Figure 2. The average measured concentration of SO_3 mostly varied from 10^4 to 10^5 molecules cm^{-3} at all locations except Mace Head where on some days SO_3 was as high as 10^7 molecules cm^{-3} (Figure 2D). The time period for Maïdo Observatory illustrated in Figure 2E pertains specifically during the volcanic eruption when SO_2 concentration at the measurement site was close to 100 ppb at its highest.[106] The prevalence of SO_3 in such diverse chemical environments suggests the hitherto unprecedented occurrence of its bimolecular reaction with other atmospherically relevant species, such as organic and inorganic acids.

3.3. Reaction of SO_3 with Monocarboxylic Acids. The reaction of monocarboxylic acids, namely, acetic acid (AA) and propionic acid (PA) with SO_3, produced acetic sulfuric anhydride (ASA) and propionic sulfuric anhydride (PSA), respectively (Figure 3A). The computed reaction rate coefficients and the energetics of the clustering pathways enabling the detection of these products by NO_3^--CIMS is provided in Table 1. These products were formed by the cycloaddition reaction mechanism of SO_3 to AA or PA, where the acidic hydrogen atom is transferred to one of the O atoms of the SO_3 molecule accompanied by a simultaneous formation of O (from acid) and S bonds (details are given in Section 3.5). Along with the CSA*NO_3^- clusters, deprotonated signals of ASA ($CH_3COOSO_3^-$) and PSA ($C_2H_5COOSO_3^-$) were also observed in our spectra. The product signal intensities showed an increasing trend when the concentrations of the acids were ramped up. With the addition of water (~10^{16} molecules cm^{-3}) to the reaction system, the signal corresponding to ASA and PSA dropped. This can be attributed to the fact that upon the addition of sufficient water, all of the SO_3 gets converted to SA and hence diminishes the product signal. This can be verified by the decrement of the SO_3 signal intensity and a corresponding increase in the SA signal intensity (Figure 3). Upon the addition of water, the signal intensity corresponding to the parent AA (or PA) increases, which is due to less consumption in the reaction with SO_3 in the system. These shreds of evidence confirm the generation of SO_3 in our reaction system and show that ASA (or PSA) is formed solely due to the reaction of SO_3 with AA (or PA). The normalized time series plot indicating the variation of the signal intensities of the products and reactants in the AA-SO_3 reaction system is shown in Figure 4, and for all other reaction systems, it is shown in the Supporting Information (Figures S8−S12). The mass spectra showing the effect of water for all of the studied reaction systems are shown in Figures S2−S7 in the Supporting Information.

3.4. Reaction of SO_3 with Dicarboxylic Acids. A similar set of experiments were performed for the reaction of SO_3 with oxalic (OA) and malonic acids (MA). In contrast to monocarboxylic acids, now there is a possibility of SO_3 addition to both carboxylic groups of the same molecule, which leads to the formation of secondary products, namely, oxalic/malonic disulfuric anhydride (ODSA/MDSA) along with the primary products, oxalic/malonic monosulfuric anhydride (OMSA/MMSA). The concentrations of the acids were increased while maintaining the same concentration of SO_2, TME, and ozone in the reaction system to verify the product signal, which shows the corresponding increase in their respective signal intensity. In the OA-SO_3 system, the deprotonated signal was observed for both OMSA and ODSA, whereas the NO_3^- cluster for ODSA was not observed. It is revealed from the spectra as well as from quantum chemical

https://doi.org/10.1021/jacs.4c04531
J. Am. Chem. Soc. 2024, 146, 15562−15575

Table 1. Calculated Rate Coefficients and Fragmentation and Deprotonation Enthalpies of the Formed Products along with Their Exact Mass-to-Charge Ratios[a]

reaction system (acid + $SO_3 \rightarrow X$)	k^b (cm^3 $molecule^{-1}$ s^{-1})	ΔH_a (kcal mol^{-1}) ($X^*NO_3^- \rightarrow X + NO_3^-$)	ΔH_b (kcal mol^{-1}) ($X^*NO_3^- \rightarrow X^- + HNO_3$)	product species	exact mass-to-charge ratio (m/z; Th)[f]
CH_3COOH (AA) + $SO_3 \rightarrow CH_3COOSO_3H$	1.37×10^{-10}	40.73	20.88	$C_2H_3O_2SO_3^-$	138.9707
				$C_2H_3O_2SO_3H^e$	201.9663
CH_3CH_2COOH (PA) + $SO_3 \rightarrow CH_3CH_2COOSO_3H$	1.60×10^{-10}	40.28	20.79	$C_3H_5O_2SO_3^-$	152.9863
				$C_3H_5O_2SO_3H^e$	215.9820
$C_2H_2O_4$ (OA) + $SO_3 \rightarrow C_2HO_4SO_3H$	9.72×10^{-12c}	50.82	17.62	$C_2HO_4SO_3^-$	168.9448
				$C_2HO_4SO_3H^e$	231.9405
$C_2HO_4SO_3H$ + $SO_3 \rightarrow C_2O_4(SO_3H)_2$	3.40×10^{-11d}	59.04	12.95	$C_2HO_4(SO_3)_2^-$	248.9017
$C_3H_4O_4$ (PA) + $SO_3 \rightarrow C_3H_3O_4SO_3H$	5.83×10^{-12c}	49.87	16.56	$C_3H_3O_4SO_3^-$	182.9605
$C_3H_3O_4SO_3H$ + $SO_3 \rightarrow C_3H_2O_4(SO_3H)_2$	7.70×10^{-12d}	51.38	12.87	$C_3H_3O_4SO_3H^e$	245.956
H_2SO_4 (SA) + $SO_3 \rightarrow H_2S_2O_7$	2.75×10^{-11}	53.18	16.72	$HS_2O_7^-$	176.9169
				$H_2S_2O_7^e$	239.9126
HIO_3 (IA) + $SO_3 \rightarrow IO_3SO_3H$	5.43×10^{-11}	51.10	21.59	$IO_3SO_3^-$	254.8466
				$IO_3SO_3H^e$	317.8422

[a]ΔH_a − fragmentation enthalpy. ΔH_b − deprotonation enthalpy. [b]Rate coefficient at 1 atm. pressure and 298 K. [c]Rate coefficient for the primary addition of SO_3. [d]Rate coefficient for the secondary addition of SO_3. [e]Peaks detected as clusters with NO_3^-. [f]Mass-to-charge ratio given in Thomson unit.

calculation (vide infra) that these CSAs are prone to deprotonation, and the signal will be more intense than its nitrate cluster. In the MA-SO_3 reaction system, we did not observe any secondary products, i.e., MDSA in both deprotonated and cluster forms. Malonic acid is prone to undergo keto−enol tautomerism, forming a distinct structural isomer with only one −C(O)OH group (i.e., the enol form). The formation of an enol form of malonic acid can be self-catalyzed and can be stabilized by water molecules.[107−109] Since the enolic form of malonic acid has only one acid functionality, the formation of MDSA could be susceptible to the formation of the enol form. It could be seen in the mass spectra of the OA-SO_3 system (Figure 3B) that the signal intensity of deprotonated ODSA is nearly 25 times lower than deprotonated OMSA and in the case of the MA-SO_3 system, the intensity of the primary product (MMSA) is itself low and therefore the secondary product, i.e., MDSA was not detected. This lower intensity of MMSA is attributed to the lower concentration of MA in the reaction system due to its lower vapor pressure and the lower rate coefficient of the reaction between MA and SO_3, which is nearly half that of the OA-SO_3 reaction system, as the detection characteristics should be similar for both MMSA and OMSA (Table 1). The mass spectra showing the product peaks resulting from the reaction of OA and MA with SO_3 are shown in Figure 3B.

3.5. Reaction of SO_3 with Inorganic Acids. We performed the experiments for the reaction of SO_3 with inorganic acids, namely, sulfuric acid (SA) and iodic acid (IA). Disulfuric acid (DSA) was formed in the reaction of SA with SO_3, and the obtained mass spectrum is shown in Figure 3C. SA was bubbled into the reaction system, and the formed DSA was observed as a deprotonated cluster with nitric acid (HNO_3*$HS_2O_7^-$) as well as in its deprotonated form ($HS_2O_7^-$). DSA signal intensity shows an increasing trend with an increase in the concentration of SA.

IA was produced in situ in the reaction system by photolysis of iodine (I_2) with subsequent reaction with ozone, which initially forms IO radical. The formed IO radical further oxidizes to higher oxides, which in the presence of OH or O_3/H_2O generates IA (HIO_3).[59,110] The detailed mechanism for the formation of iodic acid and iodous acid (HIO_2, IoA) is given in the Supporting Information (S1.4). The formed iodic acid reacts with SO_3 to form iodic sulfuric anhydride (ISA), and the obtained mass spectrum is shown in Figure 3C. As observed in all of the acid + SO_3 systems inspected here, the ISA is also detected both in its deprotonated form ($IO_3SO_3^-$) and as a cluster with NO_3-(IO_3SO_3H*NO_3^-). Interestingly, we also observed a signal corresponding to iodous sulfuric anhydride (IO_2SO_3H, IoSA) clustered to NO_3^- along with iodous acid (HIO_2, IoS), the HIO_2 being recently identified as an important contributor to iodine-related ambient particle formation events.[65,111]

To the best of our knowledge, this is the first experimental observation of gas-phase DSA, ISA, and IoSA under atmospheric pressure and room temperature. When the water was added to both the reaction systems (H_2SO_4−SO_3 and HIO_3−SO_3), the signals corresponding to DSA and ISA plummeted, indicating that the formation of these products is solely due to the reaction of SO_3 with SA and IA, respectively.

3.6. Kinetic Calculation. The addition of SO_3 is an exergonic process for all studied systems, besides oxalic acid. In all cases, they first form a reaction complex (RC) before proceeding to form the product (P) via the transition state

https://doi.org/10.1021/jacs.4c04531
J. Am. Chem. Soc. 2024, 146, 15562−15575

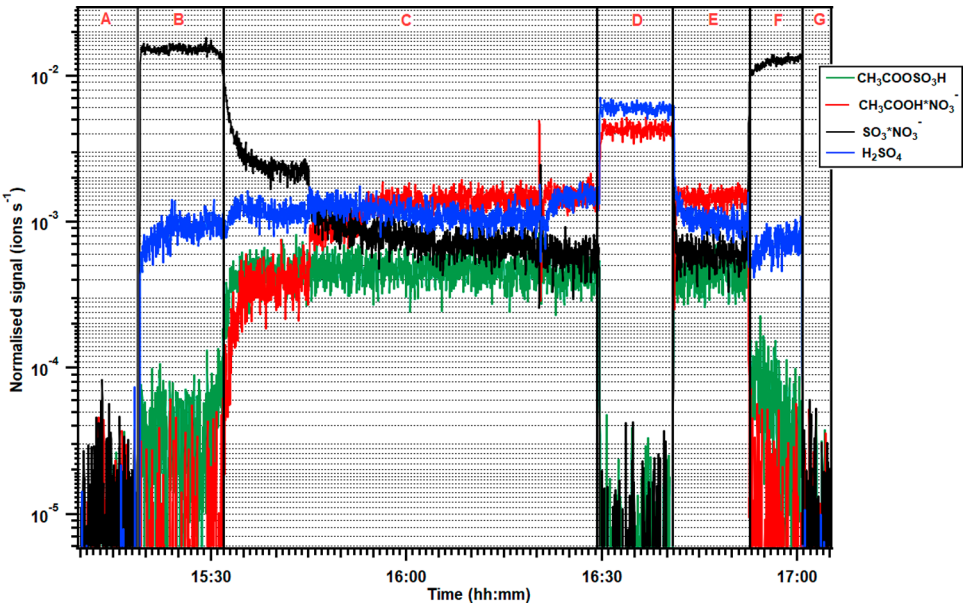

Figure 4. Normalized time series plot obtained during the reaction of acetic acid with SO_3. (A) Background; (B) injection of SO_2 and OH radical (formation of SO_3); (C) injection of acetic acid; (D) injection of water in the reaction system; (E) stopped injection of water; (F) stopped injection of acetic acid; and (G) stopped ozone (no OH radical). The normalized signals of CH_3COOSO_3H and H_2SO_4 are represented as ($S_{CH_3COOSO_3^-}$ + $S_{CH_3COOSO_3H^*NO_3^-}$) and ($S_{HSO_4^-}$ + $S_{HNO_3^*HSO_4^-}$), respectively. The concentration profile for acetic acid does not reveal its actual concentration due to the poor sensitivity of the NO_3^- reagent ion toward acetic acid.

(TS). The TS involves the migration of the acidic H atom to one of the oxygen atoms of SO_3 while simultaneously forming a bond between the carbonyl O atom of the acid and the sulfur atom. The TS structure for malonic acid is shown in Figure 5,

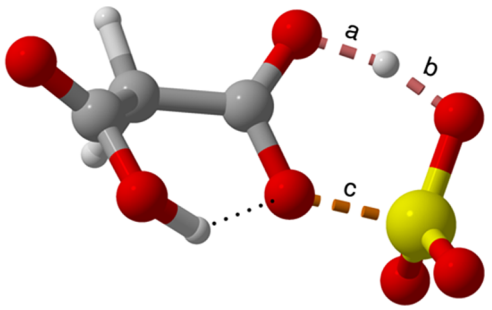

Figure 5. Transition-state geometry of malonic acid + SO_3 with the relevant bonds labeled.

Table 2. Bond Lengths of the Optimized TS Geometries and Energetics of All Stationary Points of the Studied Systems at the RHF-RCCSD(T)-F12a/VDZ-F12//ωB97X-D/aug-cc-pV(T+d)Z Level of Theory

	bond length (Å)			ΔG kcal/mol (relative to separated reactants)		
acid	*a*	*b*	*c*	RC	TS	*P*
acetic acid (AA)	1.20	1.20	1.76	−4.6	−2.5	−5.5
propionic acid (PA)	1.20	1.20	1.76	−3.9	−2.4	−6.2
oxalic acid (OA)	1.19	1.21	1.81	+2.9	+5.3	+0.4
malonic acid (MA)	1.21	1.19	1.80	+1.3	+5.1	−3.7
sulfuric acid (SA)	1.15	1.27	1.79	−0.2	+1.6	−6.0
iodic acid (IA)	1.14	1.28	1.79	−1.6	−0.9	−10.0

with the bonds participating in the reaction labeled. Table 2 shows the corresponding bond lengths of the optimized TS structure for the studied acids and the energies of all of the reaction stationary points relative to the separated reactants.

Interestingly, the studied dicarboxylic acids have significantly lower rate coefficients with SO_3 relative to the other acids, especially the monocarboxylic acids. In contrast to the monocarboxylic acids, the free dicarboxylic acid molecules have two intramolecular H-bonds instead of one. Significantly, one of the H-bonds is lost when the corresponding RC and TS structures for the studied dicarboxylic acids. This leads to higher RC and TS energies for the dicarboxylic acids compared to the other studied acids (see Figure 5), which also holds for the second SO_3 addition reaction (Table S3 in the Supporting Information). The opposite is true for the monocarboxylic acids, which have more stable RCs and lower TS energies relative to those of the dicarboxylic acids. This translates to extremely fast reactions with SO_3, with rate coefficients that are close to the collision limit. The rate coefficients of the studied inorganic acids are also very fast and lie between those of the monocarboxylic and dicarboxylic acids. Both H atoms of sulfuric acid form H-bonds with SO_3 in the RC geometry, with only one H atom transferred in the TS similar to that of the other acids. Following a similar reaction, the ISA product of iodic acid has the lowest energy relative to the separated reactants of all of the studied acids. Note that all of the studied acids react with SO_3 sufficiently fast to be relevant for atmospheric chemistry (Figure 6).

3.7. Detection of CSA, DSA, and ISA by NO_3^--CIMS.

The calculated binding enthalpies indicate that the sulfuric anhydride products form strong clusters with NO_3^- ions that are stable against fragmentation back into the reactants but can nevertheless deprotonate. This is in agreement with the observed deprotonated and cluster peaks in the NO_3^--CIMS spectra, with the former dominating for all of the studied acids. The computed enthalpies are listed in Table 1.

https://doi.org/10.1021/jacs.4c04531
J. Am. Chem. Soc. 2024, 146, 15562−15575

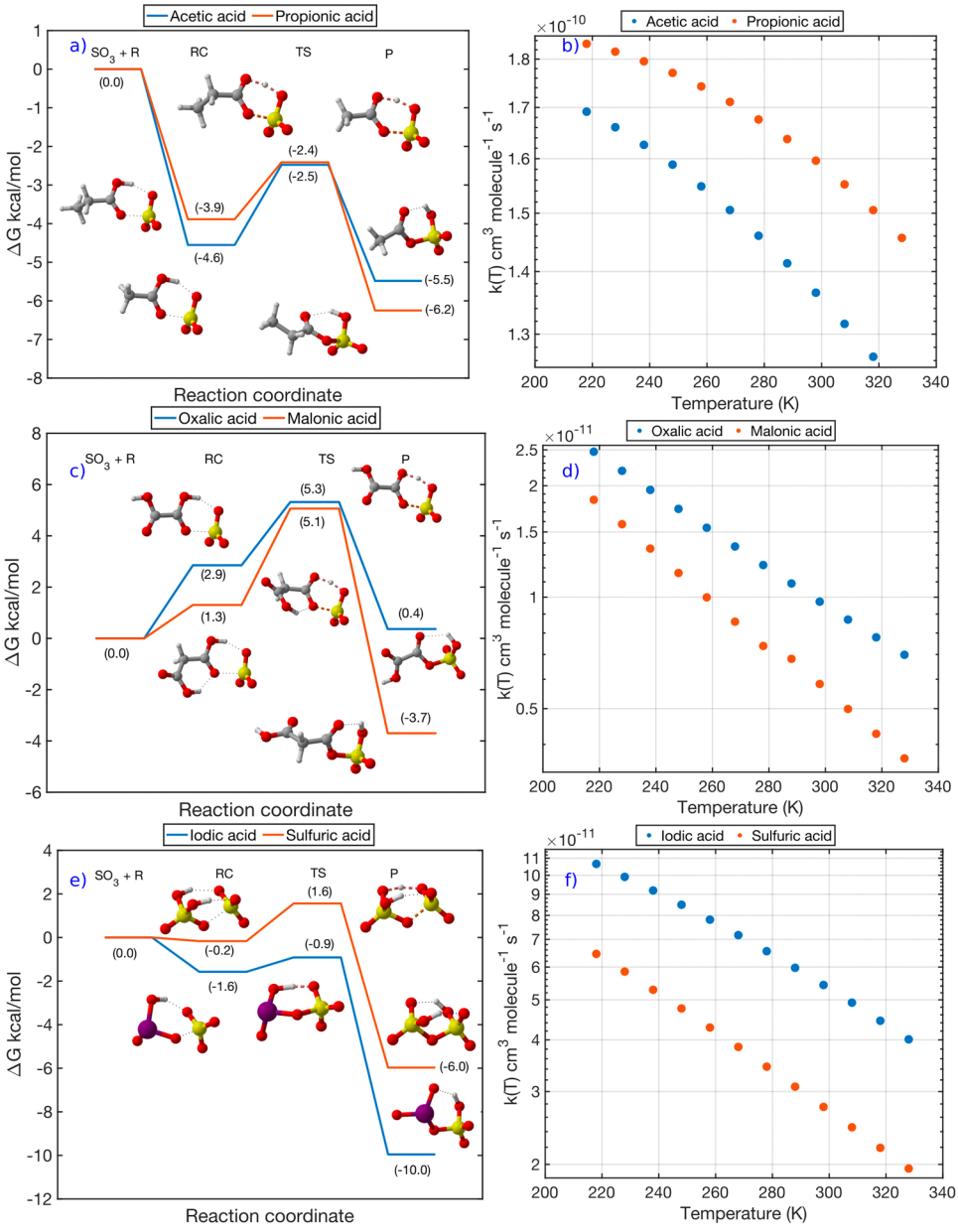

Figure 6. Potential energy surface and computationally calculated temperature-dependent rate coefficients for the bimolecular reaction of SO_3 with the studied (a, b) carboxylic acids, (c, d) dicarboxylic acids, and (e, f) inorganic acids. The energies shown in the potential energy surfaces are calculated at the RHF-RCCSD(T)-F12a/VDZ-F12//ωB97X-D/aug-cc-pV(T+d)Z level of theory. Color coding for the atoms: sulfur, yellow; oxygen, red; hydrogen, white; and iodine, purple.

3.8. Atmospheric Implications. Previous studies have indicated that the reaction of SO_3 with water dimer to form sulfuric acid is the dominant loss pathway of gaseous SO_3 in the troposphere.[112−116] The concentration of water can range from 10^{12} to 10^{17} molecules cm^{-3} under tropospheric conditions,[117] and the experimental rate coefficient for the conversion of SO_3 to SA via its reaction with water in the temperature range of 250−360 K is $(2.26 \pm 0.85) \times 10^{-43} T \exp((6544 \pm 106)/T)$ $[H_2O]^2$ s^{-1}.[114] This results in an apparent SO_3 tropospheric lifetime of only around 10^{-5} s with respect to its reaction with water dimer. We compared this to the lifetime of SO_3 with respect to its reaction with the studied acids using the temperature-dependent rate coefficients computed in this study. Table S4 (in the Supporting Information) compares the lifetime of SO_3 against its reaction with the water dimer and the studied acid molecules at RH = 20 and 40%. The calculated lifetime values indicate that the dominant loss of SO_3 is its reaction with the water dimer, with reaction with propionic acid accounting for a maximum 6% of SO_3 loss at T = 275 K. The loss of SO_3 to the remaining acids ranges from 5% to completely negligible. Despite this, we should highlight that gaseous SO_3 was nevertheless measured at concentrations above 10^6 molecules cm^{-3} during winter in Beijing, China.[73] Moreover, as shown in Figure 2, SO_3 is also detected in significant concentrations in high-altitude marine environments, volcanic plumes, urban measurement sites, and polar regions. Interestingly, the signal related to CSA, particularly, acetic sulfuric anhydride ($CH_3COOSO_3^-$), was detected in the urban region at both roadside and background measurement sites in Leipzig, Germany (Figure 7A−C), and

https://doi.org/10.1021/jacs.4c04531
J. Am. Chem. Soc. 2024, 146, 15562−15575

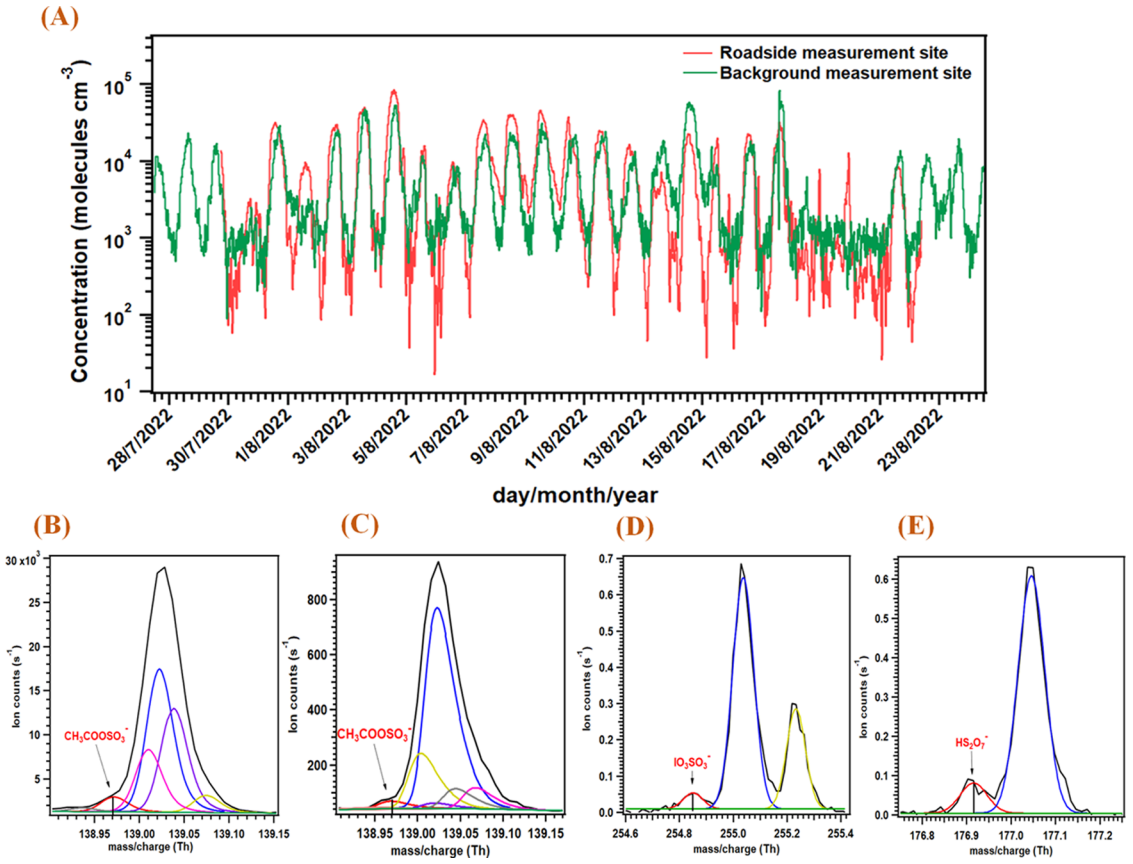

Figure 7. Time series of acetic sulfuric anhydride (deprotonated form; $CH_3COOSO_3^-$) measured at urban roadside and background sites in Leipzig, Germany (A); high-resolution peak fit of acetic sulfuric anhydride (deprotonated form; $CH_3COOSO_3^-$) measured at the urban roadside (B) and background (C) sites in Leipzig, Germany; deprotonated iodic sulfuric anhydride (ISA; $IO_3SO_3^-$) measured at Mace Head research station, Ireland (C); and deprotonated disulfuric acid (DSA; $HS_2O_7^-$) measured at Mace Head research station, Ireland (D). Black and red color traces in the spectra (B–E) represent the raw spectra and high-resolution fitted peak for the ion of interest, respectively.

ISA and DSA were detected in the marine environment at Mace Head research station, Ireland (Figure 7D,E). To the best of our knowledge, this is the first such report of the gas-phase detection of CSA, ISA, and DSA in urban and marine air samples.

The peak corresponding to SO_3 that was persistently overlooked is seen in many of our field data as shown in Figure 2. The tool of choice for many such field measurements worldwide, NO_3^--CIMS, just happens to detect SO_3 extremely well, but due to the accepted paucity of gas-phase SO_3 under ambient conditions, the peak remained unidentified (Yao et al.,[73] a notable exception). This ubiquity of SO_3 in the ambient environment indicates that there are large gaps in our understanding of its sources and sinks and makes its reactions besides those with the water dimer of paramount importance. Our kinetic calculations indicate that the reaction with SO_3 is extremely rapid for all of the studied acids and the hydrolysis of the formed CSA is likely a route of incorporation of the (small) carboxylic acids into aerosol droplets, which is consistent with the previously published speculation.[118] The CSAs have strong nucleation potential and are potential participants in new particle formation in the atmosphere.[84−89] DSA can accelerate the NPF process from SA-NH_3-based clusters, and at the air–water interface, the deprotonated DSA can accelerate particle growth by attracting gas-phase species to the liquid surface.[90] The detection of gas-phase SO_3 in the highly humid and iodine-rich air over the Mace Head Atmospheric Research Station, Ireland, is particularly significant as this allows its interplay with the major NPF precursor, iodic acid, confirming the relevance of this reaction class in marine environments and coastal mega-cities.

4. CONCLUSIONS

This work exemplifies the gas-phase reaction between sulfur trioxide, SO_3, and common atmospheric acids including mono- and dicarboxylic acids, sulfuric acid, and iodic acid to form carboxylic sulfuric anhydrides, disulfuric acid, and iodic sulfuric anhydride, respectively, under tropospheric relevant conditions of temperature and pressure. The experiments showing the formation of sulfuric anhydrides from various carboxylic acids were reported previously. However, none of the previously reported experiments measured the products at atmospheric pressure and room temperature. The theoretical rate coefficient calculations show that these reactions are competitive to the reaction of SO_3 with water dimer and should be considered as loss processes of SO_3 in the atmosphere. Our calculations show that NO_3^- ionization coupled to CIMS is a sensitive method to detect the sulfuric anhydrides, dominantly as deprotonated ions, which was also verified by our experimental investigation. The present findings also show that these acid-derived organosulfur compounds can be formed via gas-phase reactions followed by their incorporation into atmospheric nanoparticles. This has a direct relevance to understanding the atmospheric aerosol sulfur

https://doi.org/10.1021/jacs.4c04531
J. Am. Chem. Soc. 2024, 146, 15562−15575

content, which is usually considered to be formed via multiphase reactions. These reactions advance our understanding of the organic/inorganic acid-sulfur oxides interactive chemistry in the atmosphere, and the inclusion of these reactions into atmospheric chemistry models appears critical for understanding their implication to aerosol formation, especially in highly polluted regions.

■ ASSOCIATED CONTENT

Supporting Information

The Supporting Information is available free of charge at https://pubs.acs.org/doi/10.1021/jacs.4c04531.

Details about the experimental setup and the chemical system; mass spectra of all of the studied reaction systems in the presence and absence of water; site and instrumentation descriptions of all of the field measurement sites; time series profiles of all of the studied reaction systems; high-resolution peak fitting of the product signals of all of the studied reactions; high-resolution peak fitting of all of the reported ions in the ambient measurement; time series profile of ISA and DSA measured at Mace Head research station, Ireland; the energy of the stationary points involved in the secondary SO_3 addition to dicarboxylic acids; and atmospheric lifetimes (s) of SO_3 with respect to its bimolecular reaction with water dimer and studied acids in the temperature range of 275−320 K (PDF)

■ AUTHOR INFORMATION

Corresponding Authors

Avinash Kumar − *Aerosol Physics Laboratory, Physics Unit, Faculty of Engineering and Natural Sciences, Tampere University, 33720 Tampere, Finland;* orcid.org/0000-0002-8148-9252; Email: avinashkumar@tuni.fi

Siddharth Iyer − *Aerosol Physics Laboratory, Physics Unit, Faculty of Engineering and Natural Sciences, Tampere University, 33720 Tampere, Finland;* orcid.org/0000-0001-5989-609X; Email: siddharth.iyer@tuni.fi

Matti Rissanen − *Aerosol Physics Laboratory, Physics Unit, Faculty of Engineering and Natural Sciences, Tampere University, 33720 Tampere, Finland; Department of Chemistry, University of Helsinki, 00014 Helsinki, Finland;* orcid.org/0000-0003-0463-8098; Email: matti.rissanen@tuni.fi

Authors

Shawon Barua − *Aerosol Physics Laboratory, Physics Unit, Faculty of Engineering and Natural Sciences, Tampere University, 33720 Tampere, Finland;* orcid.org/0000-0003-1683-2242

James Brean − *School of Geography, Earth & Environmental Sciences, University of Birmingham, Birmingham B15 2TT, United Kingdom;* orcid.org/0000-0001-5430-6994

Emin Besic − *Aerosol Physics Laboratory, Physics Unit, Faculty of Engineering and Natural Sciences, Tampere University, 33720 Tampere, Finland*

Prasenjit Seal − *Aerosol Physics Laboratory, Physics Unit, Faculty of Engineering and Natural Sciences, Tampere University, 33720 Tampere, Finland*

Manuel Dall'Osto − *Institute of Marine Science, Consejo Superior de Investigaciones Científicas (CSIC), Barcelona 08003, Spain;* orcid.org/0000-0003-4203-894X

David C. S. Beddows − *National Centre for Atmospheric Science, School of Geography, Earth and Environmental Sciences, University of Birmingham, Birmingham B15 2TT, U.K.*

Nina Sarnela − *Institute for Atmospheric and Earth System Research (INAR)/Physics, Faculty of Science, University of Helsinki, Helsinki 00014, Finland*

Tuija Jokinen − *Institute for Atmospheric and Earth System Research (INAR)/Physics, Faculty of Science, University of Helsinki, Helsinki 00014, Finland; Climate & Atmosphere Research Centre (CARE-C), The Cyprus Institute, Nicosia 1645, Cyprus*

Mikko Sipilä − *Institute for Atmospheric and Earth System Research (INAR)/Physics, Faculty of Science, University of Helsinki, Helsinki 00014, Finland*

Roy M. Harrison − *School of Geography, Earth & Environmental Sciences, University of Birmingham, Birmingham B15 2TT, United Kingdom;* orcid.org/0000-0002-2684-5226

Complete contact information is available at: https://pubs.acs.org/10.1021/jacs.4c04531

Author Contributions

○A.K. and S.I. contributed equally to this paper.

Notes

The authors declare no competing financial interest.

■ ACKNOWLEDGMENTS

This project has received funding from the European Research Council under the European Union's Horizon 2020 research and innovation programme under Grant No. 101002728. This work is also funded by the Research Council of Finland (Grant Nos.: 331207, 336531, 346373, 353836, 355966) and the doctoral school of Faculty of Engineering and Natural Sciences, Tampere University. The Leipzig measurements were supported by the U.K. Natural Environment Research Council (grant NE/V001523/1 NPF-Urban). The authors acknowledge the tofTools team for providing the data analysis program and the CSC IT Center for Science in Espoo, Finland, for providing the computing resources.

■ REFERENCES

(1) Shammas, N. K.; Wang, L. K.; Wang, M. H. S. Sources, chemistry and control of acid rain in the environment. In *Handbook of Environment and Waste Management: Acid Rain and Greenhouse Gas Pollution Control*; World Scientific, 2020; pp 1−26.

(2) Zhang, R.; Wang, G.; Guo, S.; Zamora, M. L.; Ying, Q.; Lin, Y.; Wang, W.; Hu, M.; Wang, Y. Formation of urban fine particulate matter. *Chem. Rev.* **2015**, *115*, 3803−3855.

(3) Wang, Y. X.; Zhang, Q. Q.; Jiang, J. K.; Zhou, W.; Wang, B. Y.; He, K. B.; Duan, F. K.; Zhang, Q.; Philip, S.; Xie, Y. Y. Enhanced Sulfate Formation during China's Severe Winter Haze Episode in January 2013 Missing from Current Models. *J. Geophys. Res.: Atmos* **2014**, *119*, 10425−10440, DOI: 10.1002/2013jd021426.

(4) Engdahl, R. B. A critical review of regulations for the control of sulfur oxide emissions. *J. Air Pollut. Control Assoc.* **1973**, *23*, 364−375.

(5) Badr, O.; Probert, S. D. Atmospheric sulphur: trends, sources, sinks and environmental impacts. *Appl. Energy* **1994**, *47*, 1−67, DOI: 10.1016/0306-2619(94)90030-2.

(6) Bates, T. S.; Lamb, B. K.; Guenther, A.; Dignon, J.; Stoiber, R. E. Sulfur emissions to the atmosphere from natural sources. *J. Atmos. Chem.* **1992**, *14*, 315−337.

(7) Larssen, T.; Lydersen, E.; Tang, D. G.; He, Y.; Gao, J. X.; Liu, H. Y.; Duan, L.; Seip, H. M.; Vogt, R. D.; Mulder, J.; Shao, M.; Wang, Y.

H.; Shang, H.; Zhang, X. S.; Solberg, S.; Aas, W.; Okland, T.; Eilertsen, O.; Angell, V.; Li, Q. R.; Zhao, D. W.; Xiang, R. J.; Xiao, J. S.; Luo, J. H. Acid rain in China. *Environ. Sci. Technol.* **2006**, *40*, 418−425.
(8) Sipilä, M.; Berndt, T.; Petäjä, T.; Brus, D.; Vanhanen, J.; Stratmann, F.; Patokoski, J.; Mauldin, R. L.; Hyvarinen, A. P.; Lihavainen, H.; Kulmala, M. The Role of Sulfuric Acid in Atmospheric Nucleation. *Science* **2010**, *327*, 1243−1246.
(9) Kulmala, M.; Kontkanen, J.; Junninen, H.; Lehtipalo, K.; Manninen, H. E.; Nieminen, T.; Petajä, T.; Sipilä, M.; Schobesberger, S.; Rantala, P.; Franchin, A.; Jokinen, T.; Jarvinen, E.; Aijala, M.; Kangasluoma, J.; Hakala, J.; Aalto, P. P.; Paasonen, P.; Mikkila, J.; Vanhanen, J.; Aalto, J.; Hakola, H.; Makkonen, U.; Ruuskanen, T.; Mauldin, R. L.; Duplissy, J.; Vehkamaki, H.; Back, J.; Kortelainen, A.; Riipinen, I.; Kurten, T.; Johnston, M. V.; Smith, J. N.; Ehn, M.; Mentel, T. F.; Lehtinen, K. E.; Laaksonen, A.; Kerminen, V. M.; Worsnop, D. R. Direct observations of atmospheric aerosol nucleation. *Science* **2013**, *339*, 943−946.
(10) Yao, L.; Garmash, O.; Bianchi, F.; Zheng, J.; Yan, C.; Kontkanen, J.; Junninen, H.; Mazon, S. B.; Ehn, M.; Paasonen, P.; Sipilä, M.; Wang, M.; Wang, X.; Xiao, S.; Chen, H.; Lu, Y.; Zhang, B.; Wang, D.; Fu, Q.; Geng, F.; Li, L.; Wang, H.; Qiao, L.; Yang, X.; Chen, J.; Kerminen, V. M.; Petajä, T.; Worsnop, D. R.; Kulmala, M.; Wang, L. Atmospheric new particle formation from sulfuric acid and amines in a Chinese megacity. *Science* **2018**, *361*, 278−281.
(11) Nguyen, Q. T.; Christensen, M. K.; Cozzi, F.; Zare, A.; Hansen, A. M. K.; Kristensen, K.; Tulinius, T. E.; Madsen, H. H.; Christensen, J. H.; Brandt, J.; Massling, A.; Nøjgaard, J. K.; Glasius, M. Understanding the anthropogenic influence on formation of biogenic secondary organic aerosols in Denmark via analysis of organosulfates and related oxidation products. *Atmos. Chem. Phys.* **2014**, *14*, 8961−8981.
(12) Romero, F.; Oehme, M. Organosulfates − A new component of humic-like substances in atmospheric aerosols? *J. Atmos. Chem.* **2005**, *52*, 283−294.
(13) Riva, M.; Chen, Y.; Zhang, Y.; Lei, Z.; Olson, N. E.; Boyer, H. C.; Narayan, S.; Yee, L. D.; Green, H. S.; Cui, T.; Zhang, Z.; Baumann, K.; Fort, M.; Edgerton, E.; Budisulistiorini, S. H.; Rose, C. A.; Ribeiro, I. O.; e Oliveira, R. L.; dos Santos, E. O.; Machado, C. M. D.; Szopa, S.; Zhao, Y.; Alves, E. G.; de Sá, S. S.; Hu, W.; Knipping, E. M.; Shaw, S. L.; Duvoisin, S., Jr; de Souza, R. A. F.; Palm, B. B.; Jimenez, J. L.; Glasius, M.; Goldstein, A. H.; Pye, H. O. T.; Gold, A.; Turpin, B. J.; Vizuete, W.; Martin, S. T.; Thornton, J. A.; Dutcher, C. S.; Ault, A. P.; Surratt, J. D. Increasing Isoprene Epoxydiol-to-Inorganic Sulfate Aerosol Ratio Results in Extensive Conversion of Inorganic Sulfate to Organosulfur Forms: Implications for Aerosol Physicochemical Properties. *Environ. Sci. Technol.* **2019**, *53*, 8682−8694, DOI: 10.1021/acs.est.9b01019.
(14) Brüggemann, M.; Xu, R.; Tilgner, A.; Kwong, K. C.; Mutzel, A.; Poon, H. Y.; Otto, T.; Schaefer, T.; Poulain, L.; Chan, M. N.; Herrmann, H. Organosulfates in Ambient Aerosol: State of Knowledge and Future Research Directions on Formation, Abundance, Fate, and Importance. *Environ. Sci. Technol.* **2020**, *54*, 3767−3782.
(15) Riva, M.; Tomaz, S.; Cui, T.; Lin, Y.-H.; Perraudin, E.; Gold, A.; Stone, E. A.; Villenave, E.; Surratt, J. D. Evidence for an Unrecognized Secondary Anthropogenic Source of Organosulfates and Sulfonates: Gas-Phase Oxidation of Polycyclic Aromatic Hydrocarbons in the Presence of Sulfate Aerosol. *Environ. Sci. Technol.* **2015**, *49*, 6654−6664.
(16) Ehn, M.; Junninen, H.; Petäjä, T.; Kurtén, T.; Kerminen, V. M.; Schobesberger, S.; Manninen, H. E.; Ortega, I. K.; Vehkamäki, H.; Kulmala, M.; Worsnop, D. R. Composition and temporal behavior of ambient ions in the boreal forest. *Atmos. Chem. Phys.* **2010**, *10*, 8513−8530.
(17) Finlayson-Pitts, B. J.; Pitts, J. N., Jr. *Chemistry of the Upper and Lower Atmosphere*; Academic Press, San Diego, CA, 2000.
(18) Seinfeld, J. H.; Pandis, S. N. *Atmospheric Chemistry and Physics: From Air Pollution to Climate Change*; Wiley, New York, 1998.
(19) Rose, C.; Zha, Q.; Dada, L.; Yan, C.; Lehtipalo, K.; Junninen, H.; Mazon, S. B.; Jokinen, T.; Sarnela, N.; Sipilä, M.; Petäjä, T.; Kerminen, V. M.; Bianchi, F.; Kulmala, M. Observations of biogenic ion-induced cluster formation in the atmosphere. *Sci. Adv.* **2018**, *4*, No. eaar5218.
(20) Wang, Y. H.; Liu, Z. R.; Zhang, J. K.; Hu, B.; Ji, D. S.; Yu, Y. C.; Wang, Y. S. Aerosol physicochemical properties and implications for visibility during an intense haze episode during winter in Beijing. *Atmos. Chem. Phys.* **2015**, *15*, 3205−3215.
(21) Lee, S. H.; Gordon, H.; Yu, H.; Lehtipalo, K.; Haley, R.; Li, Y.; Zhang, R. New Particle Formation in the Atmosphere: From Molecular Clusters to Global Climate. *J. Geophys. Res.: Atmos.* **2019**, *124*, 7098−7146, DOI: 10.1029/2018JD029356.
(22) Zhang, R.; Suh, I.; Zhao, J.; Zhang, D.; Fortner, E. C.; Tie, X.; Molina, L. T.; Molina, M. J. Atmospheric New Particle Formation Enhanced by Organic Acids. *Science* **2004**, *304*, 1487−1490.
(23) Shakya, K. M.; Peltier, R. E. Investigating Missing Sources of Sulfur at Fairbanks, Alaska. *Environ. Sci. Technol.* **2013**, *47*, 9332−9338.
(24) Surratt, J. D.; Kroll, J. H.; Kleindienst, T. E.; Edney, E. O.; Claeys, M.; Sorooshian, A.; Ng, N. L.; Offenberg, J. H.; Lewandowski, M.; Jaoui, M.; Flagan, R. C.; Seinfeld, J. H. Evidence for Organosulfates in Secondary Organic Aerosol. *Environ. Sci. Technol.* **2007**, *41*, 517−527.
(25) Iinuma, Y.; Müller, C.; Berndt, T.; Böge, O.; Claeys, M.; Herrmann, H. Evidence for the Existence of Organosulfates from β-Pinene Ozonolysis in Ambient Secondary Organic Aerosol. *Environ. Sci. Technol.* **2007**, *41*, 6678−6683.
(26) Surratt, J. D.; Gómez-González, Y.; Chan, A. W.; Vermeylen, R.; Shahgholi, M.; Kleindienst, T. E.; Edney, E. O.; Offenberg, J. H.; Lewandowski, M.; Jaoui, M.; Maenhaut, W.; et al. Organosulfate formation in biogenic secondary organic aerosol. *J. Phys. Chem. A* **2008**, *112*, 8345−8378.
(27) Lukács, H.; Gelencsér, A.; Hoffer, A.; Kiss, G.; Horváth, K.; Hartyáni, Z. Quantitative assessment of organosulfates in size-segregated rural fine aerosol. *Atmos. Chem. Phys.* **2009**, *9*, 231−238.
(28) Khwaja, H. A. Atmospheric Concentrations of Carboxylic Acids and Related Compounds at a Semiurban Site. *Atmos. Environ.* **1995**, *29*, 127−139.
(29) Veres, P. R.; Roberts, J. M.; Cochran, A. K.; Gilman, J. B.; Kuster, W. C.; Holloway, J. S.; Graus, M.; Flynn, J.; Lefer, B.; Warneke, C.; de Gouw, J. Evidence of Rapid Production of Organic Acids in an Urban Air Mass. *Geophys. Res. Lett.* **2011**, *38*, No. L17807.
(30) Veres, P.; Roberts, J. M.; Burling, I. R.; Warneke, C.; de Gouw, J.; Yokelson, R. J. Measurements of Gas-Phase Inorganic and Organic Acids from Biomass Fires by Negative-Ion Proton-Transfer Chemical−Ionization Mass Spectrometry. *J. Geophys. Res.: Atmos.* **2010**, *115*, No. D23302.
(31) Kawamura, K.; Steinberg, S.; Kaplan, I. R. Homologous Series of C1 − C10 Monocarboxylic Acids and C1-C6 Carbonyls in Los Angeles Air and Motor Vehicle Exhausts. *Atmos. Environ.* **2000**, *34*, 4175−4191.
(32) Khare, P.; Kumar, N.; Kumari, K. M.; Srivastava, S. S. Atmospheric Formic and Acetic Acids: An Overview. *Rev. Geophys.* **1999**, *37*, 227−248.
(33) Helas, G.; Bingemer, H.; Andreae, M. O. Organic Acids over Equatorial Africa: Results from DECAFE 88. *J. Geophys. Res.: Atmos.* **1992**, *97*, 6187−6193.
(34) Abdullahi, K. L.; Delgado-Saborit, J. M.; Harrison, R. M. Emissions and indoor concentrations of particulate matter and its specific chemical components from cooking: A review. *Atmos. Environ.* **2013**, *71*, 260−294.
(35) Hoffmann, T.; Bandur, R.; Marggraf, U.; Linscheid, M. Molecular Composition of Organic Aerosols Formed in the α-Pinene/O3 Reaction: Implications for New Particle Formation Processes. *J. Geophys. Res.: Atmos.* **1998**, *103*, 25569−25578.
(36) Zhang, R.; Suh, I.; Zhao, J.; Zhang, D.; Fortner, E. C.; Tie, X.; Molina, L. T.; Molina, M. J. Atmospheric New Particle Formation Enhanced by Organic Acids. *Science* **2004**, *304*, 1487−1490.

(37) Winkler, P. M.; Orgeta, J.; Karl, T.; Cappellin, L.; Friedli, H. R.; Barsanti, K.; McMurry, P. H.; Smith, J. N. Identification of Biogenic Compounds Responsible for Size-Dependent Nanoparticle Growth. *Geophys. Res. Lett.* **2012**, *39*, No. L20815, DOI: 10.1029/2012gl053253.
(38) Xu, W.; Zhang, R. A Theoretical Study of Hydrated Molecular Clusters of Amines and Dicarboxylic Acids. *J. Chem. Phys.* **2013**, *139*, No. 064312.
(39) Fang, X.; Hu, M.; Shang, D.; Tang, R.; Shi, L.; Olenius, T.; Wang, Y.; Wang, H.; Zhang, Z.; Chen, S.; Yu, X.; et al. Observational evidence for the involvement of dicarboxylic acids in particle nucleation. *Environ. Sci. Technol. Lett.* **2020**, *7*, 388−394.
(40) Elm, J.; Myllys, N.; Olenius, T.; Halonen, R.; Kurten, T.; Vehkamaki, H. Formation of Atmospheric Molecular Clusters Consisting of Sulfuric Acid and C8H12O6 Tricarboxylic Acid. *Phys. Chem. Chem. Phys.* **2017**, *19*, 4877−4886.
(41) Khwaja, H. A. Atmospheric concentrations of carboxylic acids and related compounds at a semiurban site. *Atmos. Environ.* **1995**, *29*, 127−139.
(42) Tuazon, E. C.; Winer, A. M.; Pitts, J. N., Jr. Trace pollutant concentrations in a multiday smog episode in the California southcoast air basin by long path length Fourier transform infrared spectroscopy. *Environ. Sci. Technol.* **1981**, *15*, 1232−1237, DOI: 10.1021/es00092a014.
(43) Meng, Z.; Seinfeld, J. H.; Saxena, P. Gas/Aerosol Distribution of Formic and Acetic Acids. *Aerosol Sci. Technol.* **1995**, *23*, 561−578.
(44) Ho, K. F.; Lee, S. C.; Ho, S. S. H.; Kawamura, K.; Tachibana, E.; Cheng, Y.; Zhu, T. Dicarboxylic acids, ketocarboxylic acids,α-dicarbonyls, fatty acids, and benzoic acid in urban aerosols collected during the 2006 Campaign of Air Quality Research in Beijing (CAREBeijing-2006). *J. Geophys. Res.: Atmos.* **2010**, *115*, No. D19312.
(45) Martinelango, P. K.; Dasgupta, P. K.; Al-Horr, R. S. Atmospheric production of oxalic acid/oxalate and nitric acid/nitrate in the Tampa Bay airshed: Parallel pathways. *Atmos. Environ.* **2007**, *41*, 4258−4269.
(46) Nah, T.; Ji, Y.; Tanner, D. J.; Guo, H.; Sullivan, A. P.; Ng, N. L.; Weber, R. J.; Huey, L. G. Real-time measurements of gas-phase organic acids using SF_6^- chemical ionization mass spectrometry. *Atmos. Meas. Technol.* **2018**, *11*, 5087−5104.
(47) Keene, W. C.; Galloway, J. N. Considerations regarding sources for formic and acetic acids in the troposphere. *J. Geophys. Res.: Atmos.* **1986**, *91*, 14466−14474.
(48) Andreae, M. O.; Talbot, R. W.; Andreae, T. W.; Harriss, R. C. Formic and acetic acid over the Central Amazon Region, Brazil 1. Dry season. *J. Geophys. Res.: Atmos.* **1988**, *93*, 1616−1624.
(49) Yu, S. Role of organic acids (formic, acetic, pyruvic and oxalic) in the formation of cloud condensation nuclei (CCN): A review. *Atmos. Res.* **2000**, *53*, 185−217.
(50) Khan, M. A. H.; Lyons, K.; Chhantyal-Pun, R.; McGillen, M. R.; Caravan, R. L.; Taatjes, C. A.; et al. Investigating the tropospheric chemistry of acetic acid using the global 3-D chemistry transport model, STOCHEM-CRI. *J. Geophys. Res.: Atmos.* **2018**, *123*, 6267−6281.
(51) Weber, R. J.; McMurry, P. H.; Eisele, F. L.; Tanner, D. J. Measurement of Expected Nucleation Precursor Species and 3− 500 nm Diameter Particles at Mauna Loa Observatory, Hawaii. *J. Atmos. Sci.* **1995**, *52*, 2242−2257.
(52) Weber, R. J.; Marti, J. J.; McMurry, P. H.; Eisele, F. L.; Tanner, D. J.; Jefferson, A. Measured Atmospheric New Particle Formation Rates: Implications for Nucleation Mechanisms. *Chem. Eng. Commun.* **1996**, *151*, 53−64.
(53) Birmili, W.; Berresheim, H.; Plass-Dülmer, C.; Elste, T.; Gilge, S.; Wiedensohler, A.; Uhrner, U. The Hohenpeissenberg aerosol formation experiment (HAFEX): a long-term study including size-resolved aerosol, H_2SO_4, OH, and monoterpenes measurements. *Atmos. Chem. Phys.* **2003**, *3*, 361−376.
(54) Kulmala, M.; Vehkamäki, H.; Petäjä, T.; Maso, M. D.; Lauri, A.; Kerminen, V. M.; Birmili, W.; McMurry, P. H. Formation and growth rates of ultrafine atmospheric particles: a review of observations. *J. Aerosol Sci.* **2004**, *35*, 143−176, DOI: 10.1016/j.jaerosci.2003.10.003.
(55) Kulmala, M.; Petäjä, T.; Ehn, M.; Thornton, J.; Sipilä, M.; Worsnop, D. R.; Kerminen, V. M. Chemistry of Atmospheric Nucleation: On the Recent Advances on Precursor Characterization and Atmospheric Cluster Composition in Connection with Atmospheric New Particle Formation. *Annu. Rev. Phys. Chem.* **2014**, *65*, 21−37.
(56) Kuang, C.; McMurry, P. H.; McCormick, A. V.; Eisele, F. L. Dependence of nucleation rates on sulfuric acid vapor concentration in diverse atmospheric locations. *J. Geophys. Res.: Atmos.* **2008**, *113*, No. D10209.
(57) Wang, Z. B.; Hu, M.; Yue, D. L.; Zheng, J.; Zhang, R. Y.; Wiedensohler, A.; Wu, Z. J.; Nieminen, T.; Boy, M. Evaluation on the role of sulfuric acid in the mechanisms of new particle formation for Beijing case. *Atmos. Chem. Phys.* **2011**, *11*, 12663−12671.
(58) Cai, R.; Yan, C.; Yang, D.; Yin, R.; Lu, Y.; Deng, C.; Fu, Y.; Ruan, J.; Li, X.; Kontkanen, J.; Zhang, Q.; Kangasluoma, J.; Ma, Y.; Hao, J.; Worsnop, D. R.; Bianchi, F.; Paasonen, P.; Kerminen, V. M.; Liu, Y.; Wang, L.; Zheng, J.; Kulmala, M.; Jiang, J. Sulfuric acid−amine nucleation in urban Beijing. *Atmos. Chem. Phys.* **2021**, *21*, 2457−2468.
(59) Finkenzeller, H.; Iyer, S.; He, X.-C.; Simon, M.; Koenig, T. K.; Lee, C. F.; Valiev, R.; Hofbauer, V.; Amorim, A.; Baalbaki, R.; Baccarini, A.; Beck, L.; Bell, D. M.; Caudillo, L.; Chen, D.; Chiu, R.; Chu, B.; Dada, L.; Duplissy, J.; Heinritzi, M.; Kemppainen, D.; Kim, C.; Krechmer, J.; Kürten, A.; Kvashnin, A.; Lamkaddam, H.; Lee, C. P.; Lehtipalo, K.; Li, Z.; Makhmutov, V.; Manninen, H. E.; Marie, G.; Marten, R.; Mauldin, R. L.; Mentler, B.; Müller, T.; Petäjä, T.; Philippov, M.; Ranjithkumar, A.; Rörup, B.; Shen, J.; Stolzenburg, D.; Tauber, C.; Tham, Y. J.; Tomé, A.; Vazquez-Pufleau, M.; Wagner, A. C.; Wang, D. S.; Wang, M.; Wang, Y.; Weber, S. K.; Nie, W.; Wu, Y.; Xiao, M.; Ye, Q.; Zauner-Wieczorek, M.; Hansel, A.; Baltensperger, U.; Brioude, J.; Curtius, J.; Donahue, N. M.; Haddad, I. E.; Flagan, R. C.; Kulmala, M.; Kirkby, J.; Sipilä, M.; Worsnop, D. R.; Kurten, T.; Rissanen, M.; Volkamer, R. The gas-phase formation mechanism of iodic acid as an atmospheric aerosol source. *Nat. Chem.* **2023**, *15*, 129−135.
(60) Sipilä, M.; Sarnela, N.; Jokinen, T.; Henschel, H.; Junninen, H.; Kontkanen, J.; Richters, S.; Kangasluoma, J.; Franchin, A.; Perakyla, O.; Rissanen, M. P.; Ehn, M.; Vehkamaki, H.; Kurten, T.; Berndt, T.; Petaja, T.; Worsnop, D.; Ceburnis, D.; Kerminen, V. M.; Kulmala, M.; O'Dowd, C. Molecular-scale evidence of aerosol particle formation via sequential addition of HIO_3. *Nature* **2016**, *537*, 532−534.
(61) He, X.-C.; Tham, Y. J.; Dada, L.; Wang, M.; Finkenzeller, H.; Stolzenburg, D.; Iyer, S.; Simon, M.; Kurten, A.; Shen, J.; Rorup, B.; Rissanen, M.; Schobesberger, S.; Baalbaki, R.; Wang, D. S.; Koenig, T. K.; Jokinen, T.; Sarnela, N.; Beck, L. J.; Almeida, J.; Amanatidis, S.; Amorim, A.; Ataei, F.; Baccarini, A.; Bertozzi, B.; Bianchi, F.; Brilke, S.; Caudillo, L.; Chen, D.; Chiu, R.; Chu, B.; Dias, A.; Ding, A.; Dommen, J.; Duplissy, J.; El Haddad, I.; Gonzalez Carracedo, L.; Granzin, M.; Hansel, A.; Heinritzi, M.; Hofbauer, V.; Junninen, H.; Kangasluoma, J.; Kemppainen, D.; Kim, C.; Kong, W.; Krechmer, J. E.; Kvashin, A.; Laitinen, T.; Lamkaddam, H.; Lee, C. P.; Lehtipalo, K.; Leiminger, M.; Li, Z.; Makhmutov, V.; Manninen, H. E.; Marie, G.; Marten, R.; Mathot, S.; Mauldin, R. L.; Mentler, B.; Mohler, O.; Muller, T.; Nie, W.; Onnela, A.; Petaja, T.; Pfeifer, J.; Philippov, M.; Ranjithkumar, A.; Saiz-Lopez, A.; Salma, I.; Scholz, W.; Schuchmann, S.; Schulze, B.; Steiner, G.; Stozhkov, Y.; Tauber, C.; Tome, A.; Thakur, R. C.; Vaisanen, O.; Vazquez-Pufleau, M.; Wagner, A. C.; Wang, Y.; Weber, S. K.; Winkler, P. M.; Wu, Y.; Xiao, M.; Yan, C.; Ye, Q.; Ylisirnio, A.; Zauner-Wieczorek, M.; Zha, Q.; Zhou, P.; Flagan, R. C.; Curtius, J.; Baltensperger, U.; Kulmala, M.; Kerminen, V.-M.; Kurten, T.; Donahue, N. M.; Volkamer, R.; Kirkby, J.; Worsnop, D. R.; Sipilä, M. Role of iodine oxoacids in atmospheric aerosol nucleation. *Science* **2021**, *371*, 589−595.
(62) Yu, H.; Ren, L.; Huang, X.; Xie, M.; He, J.; Xiao, H. Iodine speciation and size distribution in ambient aerosols at a coastal new

particle formation hotspot in China. *Atmos. Chem. Phys.* **2019**, *19*, 4025−4039.
(63) Baccarini, A.; Karlsson, L.; Dommen, J.; Duplessis, P.; Vüllers, J.; Brooks, I. M.; Saiz-Lopez, A.; Salter, M.; Tjernström, M.; Baltensperger, U.; Zieger, P.; Schmale, J. Frequent new particle formation over the high Arctic pack ice by enhanced iodine emissions. *Nat. Commun.* **2020**, *11*, No. 4924.
(64) Baccarini, A.; Dommen, J.; Lehtipalo, K.; Henning, S.; Modini, R. L.; Gysel-Beer, M.; Baltensperger, U.; Schmale, J. Low-volatility vapors and new particle formation over the southern ocean during the antarctic circumnavigation expedition. *J. Geophys. Res.: Atmos.* **2021**, *126*, No. e2021JD035126.
(65) He, X.-C.; Simon, M.; Iyer, S.; Xie, H.-B.; Rörup, B.; Shen, J.; Finkenzeller, H.; Stolzenburg, D.; Zhang, R.; Baccarini, A.; Tham, Y. J.; Wang, M.; Amanatidis, S.; Piedehierro, A. A.; Amorim, A.; Baalbaki, R.; Brasseur, Z.; Caudillo, L.; Chu, B.; Dada, L.; Duplissy, J.; Haddad, I. E.; Flagan, R. C.; Granzin, M.; Hansel, A.; Heinritzi, M.; Hofbauer, V.; Jokinen, T.; Kemppainen, D.; Kong, W.; Krechmer, J.; Kürten, A.; Lamkaddam, H.; Lopez, B.; Ma, F.; Mahfouz, N. G. A.; Makhmutov, V.; Manninen, H. E.; Marie, G.; Marten, R.; Massabò, D.; Mauldin, R. L.; Mentler, B.; Onnela, A.; Petäjä, T.; Pfeifer, J.; Philippov, M.; Ranjithkumar, A.; Rissanen, M. P.; Schobesberger, S.; Scholz, W.; Schulze, B.; Surdu, M.; Thakur, R. C.; Tomé, A.; Wagner, A. C.; Wang, D.; Wang, Y.; Weber, S. K.; Welti, A.; Winkler, P. M.; Wieczorek, M. Z.; Baltensperger, U.; Curtius, J.; Kurtén, T.; Worsnop, D. R.; Volkamer, R.; Lehtipalo, K.; Kirkby, J.; Donahue, N. M.; Sipilä, M.; Kulmala, M. Iodine oxoacids enhance nucleation of sulfuric acid particles in the atmosphere. *Science* **2023**, *382*, 1308−1314.
(66) Yin, K.; Mai, S.; Zhao, J. Atmospheric Sulfuric Acid Dimer Formation in a Polluted Environment. *Int. J. Environ. Res. Public Health* **2022**, *19*, No. 6848.
(67) Beck, L. J.; Schobesberger, S.; Sipilä, M.; Kerminen, V. M.; Kulmala, M. Estimation of sulfuric acid concentration using ambient ion composition and concentration data obtained with atmospheric pressure interface time-of-flight ion mass spectrometer. *Atmos. Meas. Technol.* **2022**, *15*, 1957−1965.
(68) Dada, L.; Ylivinkka, I.; Baalbaki, R.; Li, C.; Guo, Y.; Yan, C.; Yao, L.; Sarnela, N.; Jokinen, T.; Daellenbach, K. R.; Yin, R.; et al. Sources and sinks driving sulfuric acid concentrations in contrasting environments: implications on proxy calculations. *Atmos. Chem. Phys.* **2020**, *20* (20), 11747−11766.
(69) Jokinen, T.; Sipilä, M.; Junninen, H.; Ehn, M.; Lönn, G.; Hakala, J.; Petäjä, T.; Mauldin, R. L., III; Kulmala, M.; Worsnop, D. R. Atmospheric sulphuric acid and neutral cluster measurements using CI-APi-TOF. *Atmos. Chem. Phys.* **2012**, *12*, 4117−4125.
(70) Zhang, Y.; Li, D.; He, X.-C.; Nie, W.; Deng, C.; Cai, R.; Liu, Y.; Guo, Y.; Liu, C.; Li, Y.; Chen, L.; Li, Y.; Hua, C.; Liu, T.; Wang, Z.; Xie, J.; Wang, L.; Petäjä, T.; Bianchi, F.; Qi, X.; Chi, X.; Paasonen, P.; Liu, Y.; Yan, C.; Jiang, J.; Ding, A.; Kulmala, M. Iodine oxoacids and their roles in sub-3 nm particle growth in polluted urban environments. *Atmos. Chem. Phys.* **2024**, *24*, 1873−1893.
(71) Sipilä, M.; Sarnela, N.; Jokinen, T.; Henschel, H.; Junninen, H.; Kontkanen, J.; Richters, S.; Kangasluoma, J.; Franchin, A.; Peräkylä, O.; Rissanen, M. P.; Ehn, M.; Vehkamäki, H.; Kurten, T.; Berndt, T.; Petäjä, T.; Worsnop, D.; Ceburnis, D.; Kerminen, V. M.; Kulmala, M.; O'Dowd, C. Molecular-scale evidence of aerosol particle formation via sequential addition of HIO_3. *Nature* **2016**, *537*, 532−534.
(72) Thakur, R. C.; Dada, L.; Beck, L. J.; Quéléver, L. L. J.; Chan, T.; Marbouti, M.; He, X. C.; Xavier, C.; Sulo, J.; Lampilahti, J.; Lampimäki, M.; Tham, Y. J.; Sarnela, N.; Lehtipalo, K.; Norkko, A.; Kulmala, M.; Sipilä, M.; Jokinen, T. An evaluation of new particle formation events in Helsinki during a Baltic Sea cyanobacterial summer bloom. *Atmos. Chem. Phys.* **2022**, *22*, 6365−6391.
(73) Yao, L.; Fan, X.; Yan, C.; Kurtén, T.; Daellenbach, K. R.; Li, C.; Wang, Y.; Guo, Y.; Dada, L.; Rissanen, M. P.; Cai, J.; et al. Unprecedented ambient sulfur trioxide (SO_3) detection: Possible formation mechanism and atmospheric implications. *Environ. Sci. Technol. Lett.* **2020**, *7*, 809−818.
(74) Mackenzie, R. B.; Dewberry, C. T.; Leopold, K. R. Gas Phase Observation and Microwave Spectroscopic Characterization of Formic Sulfuric Anhydride. *Science* **2015**, *349*, 58−61.
(75) Huff, A. K.; Mackenzie, R. B.; Smith, C. J.; Leopold, K. R. Facile formation of acetic sulfuric anhydride: Microwave spectrum, internal rotation, and theoretical calculations. *J. Phys. Chem. A* **2017**, *121*, 5659−5664.
(76) Smith, C. J.; Huff, A. K.; Mackenzie, R. B.; Leopold, K. R. Observation of two conformers of acrylic sulfuric anhydride by microwave spectroscopy. *J. Phys. Chem. A* **2017**, *121*, 9074−9080.
(77) Huff, A. K.; Mackenzie, R. B.; Smith, C. J.; Leopold, K. R. A Perfluorinated Carboxylic Sulfuric Anhydride: Microwave and Computational Studies of CF_3COOSO_2OH. *J. Phys. Chem. A* **2019**, *123*, 2237−2243.
(78) Smith, C. J.; Huff, A. K.; Ward, R. M.; Leopold, K. R. Carboxylic Sulfuric Anhydrides. *J. Phys. Chem. A* **2020**, *124*, 601−612.
(79) Love, N.; Carpenter, C. A.; Huff, A. K.; Douglas, C. J.; Leopold, K. R. Microwave and Computational Study of Pivalic Sulfuric Anhydride and the Pivalic Acid Monomer: Mechanistic Insights into the RCOOH+ SO_3 Reaction. *J. Phys. Chem. A* **2022**, *126*, 6194−6202.
(80) Liu, L.; Zhong, J.; Vehkamäki, H.; Kurtén, T.; Du, L.; Zhang, X.; Francisco, J. S.; Zeng, X. C. Unexpected quenching effect on new particle formation from the atmospheric reaction of methanol with SO_3. *Proc. Natl. Acad. Sci. U.S.A.* **2019**, *116*, 24966−24971.
(81) Li, H.; Zhong, J.; Vehkamaki, H.; Kurtén, T.; Wang, W.; Ge, M.; Zhang, S.; Li, Z.; Zhang, X.; Francisco, J. S.; Zeng, X. C. Self-catalytic reaction of SO_3 and NH_3 to produce sulfamic acid and its implication to atmospheric particle formation. *J. Am. Chem. Soc.* **2018**, *140*, 11020−11028.
(82) Sarkar, S.; Oram, B. K.; Bandyopadhyay, B. Influence of ammonia and water on the fate of sulfur trioxide in the troposphere: theoretical investigation of sulfamic acid and sulfuric acid formation pathways. *J. Phys. Chem. A* **2019**, *123*, 3131−3141.
(83) Long, B.; Xia, Y.; Bao, J. L.; Carmona-García, J.; Gómez Martín, J. C.; Plane, J. M.; Saiz-Lopez, A.; Roca-Sanjuán, D.; Francisco, J. S. Reaction of SO_3 with $HONO_2$ and Implications for Sulfur Partitioning in the Atmosphere. *J. Am. Chem. Soc.* **2022**, *144*, 9172−9177.
(84) Yang, Y.; Liu, L.; Wang, H.; Zhang, X. Molecular-Scale Mechanism of Sequential Reaction of Oxalic Acid with SO_3: Potential Participator in Atmospheric Aerosol Nucleation. *J. Phys. Chem. A* **2021**, *125*, 4200−4208.
(85) Rong, H.; Liu, L.; Liu, J.; Zhang, X. Glyoxylic sulfuric anhydride from the gas-phase reaction between glyoxylic acid and SO_3: a potential nucleation precursor. *J. Phys. Chem. A* **2020**, *124*, 3261−3268.
(86) Zhang, H.; Wang, W.; Pi, S.; Liu, L.; Li, H.; Chen, Y.; Zhang, Y.; Zhang, X.; Li, Z. Gas phase transformation from organic acid to organic sulfuric anhydride: Possibility and atmospheric fate in the initial new particle formation. *Chemosphere* **2018**, *212*, 504−512.
(87) Zhang, H.; Wang, W.; Li, H.; Gao, R.; Xu, Y. A theoretical study on the formation mechanism of carboxylic sulfuric anhydride and its potential role in new particle formation. *RSC Adv.* **2022**, *12*, 5501−5508.
(88) Zhang, X.; Lian, Y.; Tan, S.; Yin, S. Organosulfate Produced from Consumption of SO_3 Speeds up Sulfuric Acid-Dimethylamine Atmospheric Nucleation. *EGUsphere* **2023**, 1−27.
(89) Zhang, H.; Gao, R.; Li, H.; Li, Y.; Xu, Y.; Chai, F. Formation mechanism of typical aromatic sulfuric anhydrides and their potential role in atmospheric nucleation process. *J. Environ. Sci.* **2023**, *123*, 54−64.
(90) Wang, R.; Cheng, Y.; Hu, Y.; Chen, S.; Guo, X.; Song, F.; Li, H.; Zhang, T. Reaction of SO_3 with H_2SO_4 and Its Implication for Aerosol Particle Formation in the Gas Phase and at the Air-Water Interface. *EGUsphere* **2023**, 1−31.
(91) Junninen, H.; Ehn, M.; Petäjä, T.; Luosujärvi, L.; Kotiaho, T.; Kostiainen, R.; Rohner, U.; Gonin, M.; Fuhrer, K.; Kulmala, M.; Worsnop, D. R. A high-resolution mass spectrometer to measure

atmospheric ion composition. *Atmos. Meas. Technol.* **2010**, *3*, 1039−1053.
(92) *Spartan'18*; Wavefunction Inc.: Irvine CA, 2018.
(93) *Spartan'20*; Wavefunction Inc.: Irvine CA, 2020.
(94) Møller, K. H.; Otkjær, R. V.; Hyttinen, N.; Kurtén, T.; Kjaergaard, H. G. Cost-effective implementation of multi- conformer transition state theory for peroxy radical hydro- gen shift reactions. *J. Phys. Chem. A* **2016**, *120*, 10072−10087.
(95) Frisch, M. J.; Trucks, G. W.; Schlegel, H. B.; Scuseria, G. E.; Robb, M. A.; Cheeseman, J. R.; Scalmani, G.; Barone, V.; Petersson, G. A.; Nakatsuji, H.; Li, X.; Caricato, M.; Marenich, A. V.; Bloino, J.; Janesko, B. G.; Gomperts, R.; Mennucci, B.; Hratchian, H. P.; Ortiz, J. V.; Izmaylov, A. F.; Sonnenberg, J. L.; Williams-Young, D.; Ding, F.; Lipparini, F.; Egidi, F.; Goings, J.; Peng, B.; Petrone, A.; Henderson, T.; Ranasinghe, D.; Zakrzewski, V. G.; Gao, J.; Rega, N.; Zheng, G.; Liang, W.; Hada, M.; Ehara, M.; Toyota, K.; Fukuda, R.; Hasegawa, J.; Ishida, M.; Nakajima, T.; Honda, Y.; Kitao, O.; Nakai, H.; Vreven, T.; Throssell, K.; Montgomery, J. A., Jr.; Peralta, J. E.; Ogliaro, F.; Bearpark, M. J.; Heyd, J. J.; Brothers, E. N.; Kudin, K. N.; Staroverov, V. N.; Keith, T. A.; Kobayashi, R.; Normand, J.; Raghavachari, K.; Rendell, A. P.; Burant, J. C.; Iyengar, S. S.; Tomasi, J.; Cossi, M.; Millam, J. M.; Klene, M.; Adamo, C.; Cammi, R.; Ochterski, J. W.; Martin, R. L.; Morokuma, K.; Farkas, O.; Foresman, J. B.; Fox, D. J. *Gaussian 16*, Revision B.01; Gaussian, Inc.: Wallingford, CT, 2016.
(96) Minenkov, Y.; Wang, H.; Wang, Z.; Sarathy, S. M.; Cavallo, L. Heats of formation of medium-sized organic compounds from contemporary electronic structure methods. *J. Chem. Theory Comput.* **2017**, *13*, 3537−3560.
(97) Glowacki, D. R.; Liang, C. H.; Morley, C.; Pilling, M. J.; Robertson, S. H. MESMER: an opensource master equation solver for multi-energy well reactions. *J. Phys. Chem. A* **2012**, *116*, 9545−9560.
(98) Cox, R. A.; Ammann, M.; Crowley, J. N.; Herrmann, H.; Jenkin, M. E.; McNeill, V. F.; Mellouki, A.; Troe, J.; Wallington, T. J. Evaluated kinetic and photochemical data for atmospheric chemistry: Volume VII−Criegee intermediates. *Atmos. Chem. Phys.* **2020**, *20*, 13497−13519.
(99) Drozd, G. T.; Donahue, N. M. Pressure dependence of stabilized Criegee intermediate formation from a sequence of alkenes. *J. Phys. Chem. A* **2011**, *115*, 4381−4387.
(100) Calvert, J. G.; Lazrus, A.; Kok, G. L.; Heikes, B. G.; Walega, J. G.; Lind, J.; Cantrell, C. A. Chemical mechanisms of acid generation in the troposphere. *Nature* **1985**, *317*, 27−35.
(101) Tyndall, G. S.; Ravishankara, A. R. Atmospheric oxidation of reduced sulfur species. *Int. J. Chem. Kinet.* **1991**, *23*, 483−527.
(102) Carmona-García, J.; Trabelsi, T.; Frances-Monerris, A.; Cuevas, C. A.; Saiz-Lopez, A.; Roca-Sanjuan, D.; Francisco, J. S. Photochemistry of $HOSO_2$ and SO_3 and implications for the production of sulfuric acid. *J. Am. Chem. Soc.* **2021**, *143*, 18794−18802.
(103) Berndt, T.; Jokinen, T.; Mauldin, R. L., III; Petaja, T.; Herrmann, H.; Junninen, H.; Paasonen, P.; Worsnop, D. R.; Sipila, M. Gas-phase ozonolysis of selected olefins: The yield of stabilized Criegee intermediate and the reactivity toward SO_2. *J. Phys. Chem. Lett.* **2012**, *3*, 2892−2896.
(104) De Laeter, J. R.; Böhlke, J. K.; De Bievre, P.; Hidaka, H.; Peiser, H. S.; Rosman, K. J. R.; Taylor, P. D. P. Atomic weights of the elements. Review 2000 (IUPAC Technical Report). *Pure Appl. Chem.* **2003**, *75*, 683−800.
(105) Hyttinen, N.; Kupiainen-Määttä, O.; Rissanen, M. P.; Muuronen, M.; Ehn, M.; Kurtén, T. Modeling the Charging of Highly Oxidized Cyclohexene Ozonolysis Products Using Nitrate-Based Chemical Ionization. *J. Phys. Chem. A* **2015**, *119*, 6339−6345.
(106) Rose, C.; Rissanen, M. P.; Iyer, S.; Duplissy, J.; Yan, C.; Nowak, J. B.; Colomb, A.; Dupuy, R.; He, X. C.; Lampilahti, J.; Tham, Y. J. Investigation of several proxies to estimate sulfuric acid concentration under volcanic plume conditions. *Atmos. Chem. Phys.* **2021**, *21*, 4541−4560.
(107) Ghorai, S.; Laskin, A.; Tivanski, A. V. Spectroscopic evidence of keto− enol tautomerism in deliquesced malonic acid particles. *J. Phys. Chem. A* **2011**, *115*, 4373−4380.
(108) Sutton, C. C.; Lim, C. Y.; da Silva, G. Self-catalyzed keto-enol tautomerization of malonic acid. *Int. J. Quantum Chem.* **2020**, *120*, No. e26114.
(109) García, M. P.; Windus, T. L. Computational Study of the Malonic Acid Tautomerization Products in Highly Concentrated Particles. *J. Phys. Chem. A* **2017**, *121*, 2259−2264.
(110) Plane, J. M. C.; Joseph, D. M.; Allan, B. J.; Ashworth, S. H.; Francisco, J. S. An experimental and theoretical study of the reactions OIO + NO and OIO + OH. *J. Phys. Chem. A* **2006**, *110*, 93−100.
(111) Zu, H.; Zhang, S.; Li, S.; Liu, L.; Zhang, X. 2023. The synergistic nucleation of iodous acid and sulfuric acid: A vital mechanism in polluted marine regions. *Atmos. Environ.* **2024**, *318*, No. 120266.
(112) Morokuma, K.; Muguruma, C. Ab initio molecular orbital study of the mechanism of the gas phase reaction SO_3+ H_2O: Importance of the second water molecule. *J. Am. Chem. Soc.* **1994**, *116*, 10316−10317.
(113) Kolb, C. E.; Jayne, J. T.; Worsnop, D. R.; Molina, M. J.; Meads, R. F.; Viggiano, A. A. 1994. Gas phase reaction of sulfur trioxide with water vapor. *J. Am. Chem. Soc.* **1994**, *116*, 10314−10315.
(114) Lovejoy, E. R.; Hanson, D. R.; Huey, L. G. Kinetics and products of the gas-phase reaction of SO_3 with water. *J. Phys. Chem. A* **1996**, *100*, 19911−19916.
(115) Jayne, J. T.; Pöschl, U.; Chen, Y.-m.; Dai, D.; Molina, L. T.; Worsnop, D. R.; Kolb, C. E.; Molina, M. J. Pressure and temperature dependence of the gas-phase reaction of SO_3 with H_2O and the heterogeneous reaction of SO_3 with H_2O/H_2SO_4 surfaces. *J. Phys. Chem. A* **1997**, *101*, 10000−10011.
(116) Long, B.; Xia, Y.; Zhang, Y. Q.; Truhlar, D. G. Kinetics of Sulfur Trioxide Reaction with Water Vapor to Form Atmospheric Sulfuric Acid. *J. Am. Chem. Soc.* **2023**, *145*, 19866−19876.
(117) Brasseur, G. P.; Solomon, S. *Aeronomy of the Middle Atmosphere: Chemistry and Physics of the Stratosphere and Mesosphere*; Springer Science & Business Media, 2006; pp 617−662.
(118) Smith, C. J.; Huff, A. K.; Mackenzie, R. B.; Leopold, K. R. Hydration of an Acid Anhydride: The Water Complex of Acetic Sulfuric Anhydride. *J. Phys. Chem. A* **2018**, *122*, 4549−4554.

https://doi.org/10.1021/jacs.4c04531
J. Am. Chem. Soc. 2024, 146, 15562−15575